POLITECNICO
MILANO 1863

SCUOLA DI INGEGNERIA INDUSTRIALE
E DELL'INFORMAZIONE

From Recognition to Remediation: Cellulose Nanosponges for Smart Water Purification

TESI DI LAUREA MAGISTRALE IN
CHEMICAL ENGINEERING
INGEGNERIA CHIMICA

Author: **Letizia Del Vitto**

Student ID: 10738272
Advisor: Dr. Laura Riva
Co-advisor: Dr. Arianna De Santis, Prof. Carlo Punta, Dr. Fabrizio Caroleo
Academic Year: 2024-2025

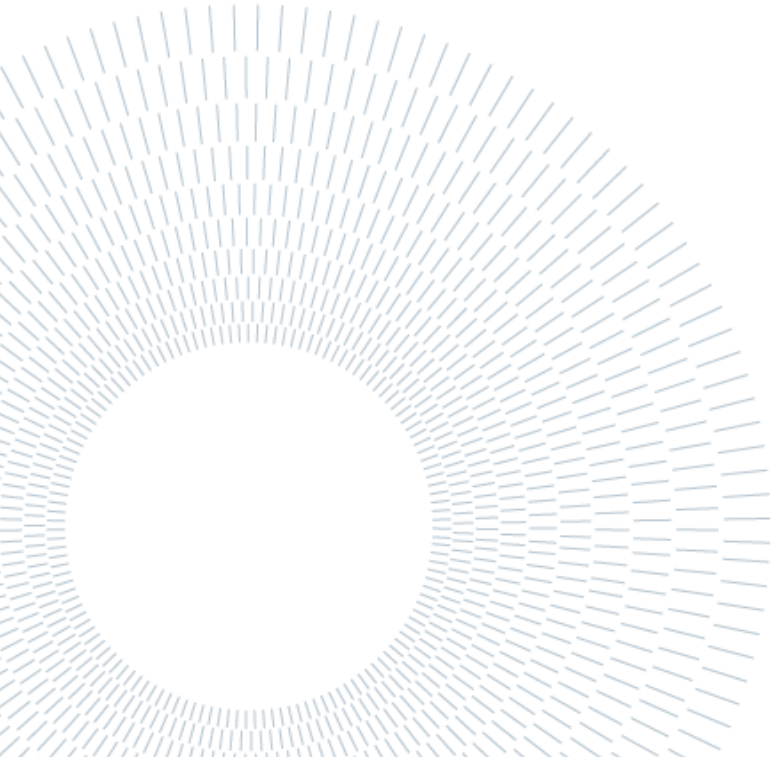

Abstract

In recent years, environmental pollution has gained increasing global attention. Especially, after the implementation of Agenda 2030 Sustainable Goals, the importance of clean water resources has become a major goal. Despite all efforts made, water is still polluted with persistent and toxic contaminants. Among all contaminants, mercury and per- and poly- fluorinated substances (PFAS) represent a critical concern due to their toxicity, environmental persistence and bioaccumulation potential. The development of sustainable and effective materials for detection and adsorption of these contaminants is necessary.

This work focuses on the development and optimization of cellulose-based nanostructured xerogels designed for the simultaneous adsorption and detection of aquatic contaminants. The research was conducted through a collaboration between the *Organic Synthesis, Catalysis and Materials Laboratory (*O^{SCM} Lab*)* at Politecnico di Milano and the *Sensor Group* at the University of Rome "Tor Vergata".

Cellulose nanosponges are composed of functionalized cellulose nanofibers, obtained through TEMPO-mediated oxidation combined with mechanical treatments, and different cross-linkers, capable of enhancing structural stability and integrity of the material. To introduce sensing capability, the nanostructured materials were functionalized with porphyrinic moieties. The incorporation of porphyrins enabled optical monitoring of contaminant uptake through colorimetric variation, allowing real-time visual detection of pollutant saturation.

Different functionalization strategies were investigated to optimize both adsorption efficiency and sensing performance. The synthesized materials were characterized through SEM and ICP analyses to evaluate their morphology and functionalization degree.

Adsorption tests demonstrated that both functionalized and pristine nanosponges exhibit a significant adsorption capacity toward mercury in aqueous solutions. Building on this evidence, the materials were further considered as potential capping agents for the remediation of contaminated marine sediments, where their ability to immobilize pollutants could be advantageously exploited. Given the large material volumes required for such environmental applications, a preliminary assessment of the scalability of the synthesis process was also undertaken to evaluate the feasibility of up-scaling the production of cellulose-based nanosponges.

Key-words: Cellulose, TEMPO-oxidation, porphyrins, adsorption, detection, mercury, PFAS.

Abstract in italiano

Negli ultimi anni, l'inquinamento ambientale ha guadagnato una crescente attenzione globale. In particolare, dopo l'introduzione degli Obiettivi Sostenibili dell'Agenda 2030, l'importanza di pulite risorse idriche è diventata un obiettivo importante. Nonostante tutte le azioni compiute, l'acqua è ancora inquinata da contaminanti persistenti e tossici. Tra tutti gli inquinanti, il mercurio e le sostanze perfluorurate e polifluorurate (PFAS) rappresentano un problema cruciale a causa della loro tossicità, persistenza ambientale e potenziale bioaccumulo. È necessario lo sviluppo di materiali sostenibili ed efficaci per il rilevamento e l'assorbimento di questi contaminanti.

Questo lavoro si concentra sullo sviluppo e l'ottimizzazione di aerogel nanostrutturati a base di cellulosa, progettati per l'adsorbimento e il rilevamento contemporaneo di contaminanti acquatici. La ricerca è stata condotta attraverso una collaborazione tra il *Organic Synthesis, Catalysis and Materials Laboratory* (O^{SCM} Lab) del Politecnico di Milano e il *Sensor Group* dell'Università di Roma "Tor Vergata".

Le nanospugne di cellulosa sono composte da nanofibre di cellulosa, ottenute tramite TEMPO-ossidazione in combinazione con trattamenti meccanici, e da diversi cross-linkers, in grado di migliorare la stabilità strutturale e l'integrità del materiale. Per introdurre la capacità di rilevamento, i materiali sono stati funzionalizzati con molecole porfiriniche. L'incorporazione di porfirine ha consentito il monitoraggio ottico dell'assorbimento dei contaminanti attraverso la variazione colorimetrica, consentendo il rilevamento visivo in tempo reale della saturazione degli inquinanti.

Sono state studiate diverse strategie di funzionalizzazione per ottimizzare sia l'efficienza di adsorbimento sia le prestazioni di rilevamento. I materiali sintetizzati sono stati caratterizzati mediante analisi SEM e ICP per valutarne la morfologia e il grado di funzionalizzazione.

I test di adsorbimento hanno dimostrato che sia le nanospugne funzionalizzate sia quelle non funzionalizzate presentano una significativa capacità di adsorbimento nei confronti del mercurio in soluzione acquosa. Sulla base di queste evidenze, i materiali sono stati quindi considerati come potenziali agenti di capping per la bonifica di sedimenti marini contaminati, ambito in cui la loro capacità di immobilizzare gli inquinanti potrebbe essere efficacemente sfruttata. Considerati i grandi quantitativi di materiale richiesti per tali applicazioni ambientali, è stata inoltre condotta una valutazione preliminare della scalabilità del processo di sintesi, al fine di verificare la fattibilità di un aumento di scala nella produzione delle nanospugne a base di cellulosa.

Parole chiave: Cellulosa, TEMPO-ossidazione, porfirine, assorbimento, rilevamento, mercurio, PFAS.

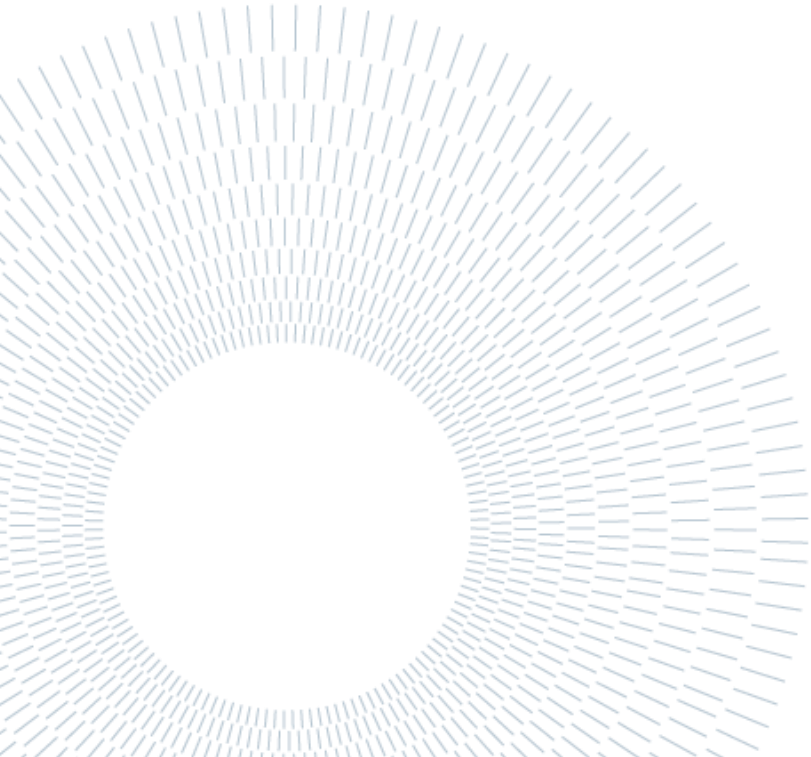

Contents

1 Introduction

1.1. Environmental problem

Environmental pollution is one the major challenges in the modern society. Indeed the 2030 Agenda for Sustainable Development, adopted by United Nations (UN) in 2015, expresses a global action plan for a more sustainable future. [1]

Figure 1: 2030 Agenda for Sustainable Development [1]

Among all the Sustainable Development Goals, particular focus is given to water and aquatic ecosystems. Goal 6 discusses the importance of clean drinking water and sanitation for all humans to prevent diseases. Similarly, Goal 14 focuses on conserving the world's oceans, seas and marine ecosystems. Both goals promote reducing pollution into freshwater and oceans, protecting the ecosystems and habitats.

Despite the global efforts, water resources are increasingly at risk by the release of persistent and toxic contaminants. Among these pollutants, heavy metals concentrations have been rising due to increasing anthropogenic activities [2]. Their toxicity and persistence in the environment are concern for human health.

Among heavy metals, mercury is one of the most toxic heavy metals present. After the Minamata disaster in 1956, mercury poisoning gained worldwide attention. The Minamata Convention was established with the aim of lower mercury levels, eliminate mercury-containing products and regulate mercury's emissions to air, water and soil [3]. Similarly, the Mediterranean Action Plan (MAP) was designed in Barcellona Convention in 1976, for the same purposes in the Mediterranean Sea [4] [5]. However, mercury concentration is still extremely high especially in water bodies and frequently exceeds law limits. [6]

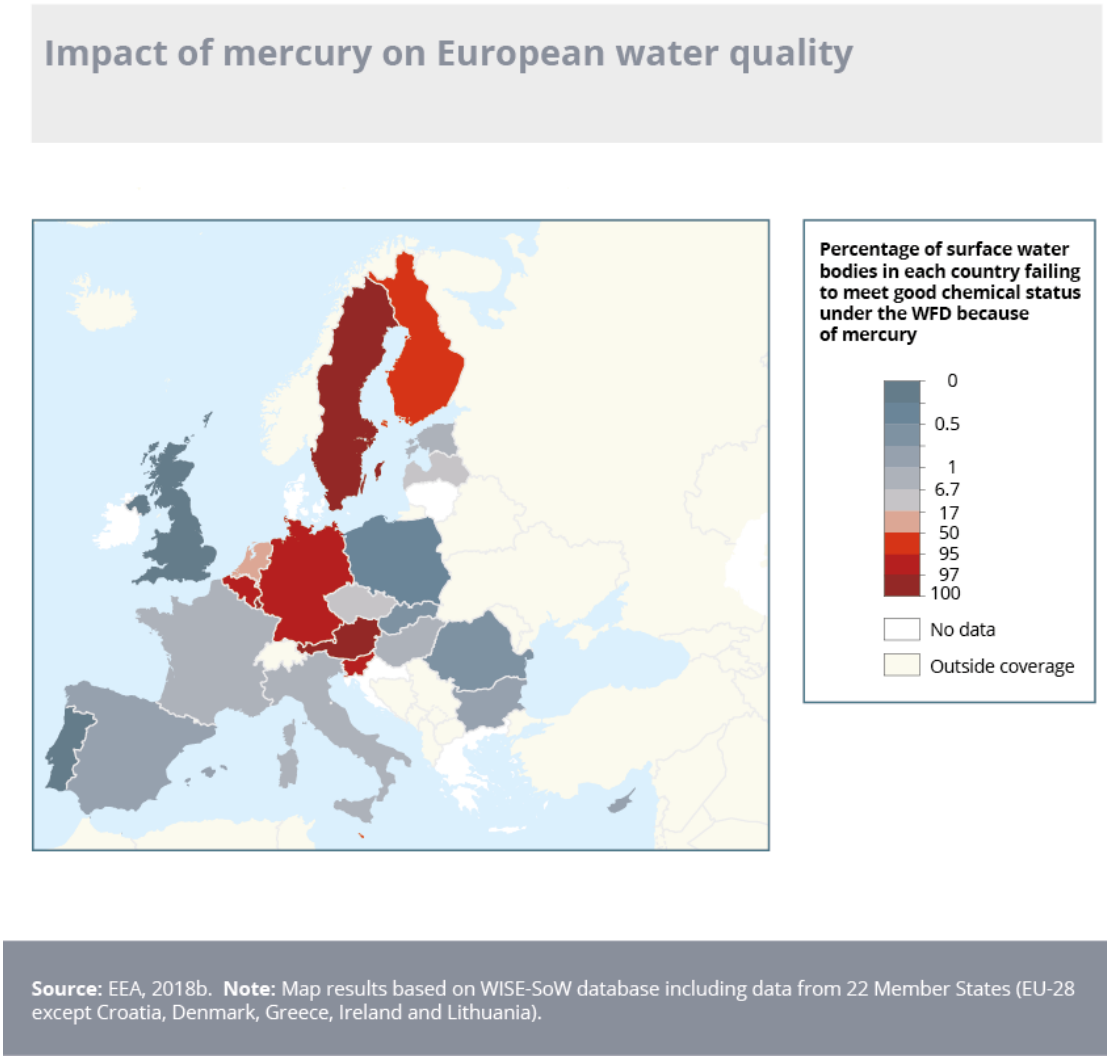

Figure 1: Mercury concentration in EU water [6]

In addition to heavy metals, per- and polyfluoroalkyl substances (PFAS) are another major source of water contamination. In particular, their persistence and bioaccumulation properties, as well as the potential to travel with either water streams or sediments, contributes to their environmental distribution [7]. Humans are mainly exposed to PFAS through drinking contaminated water, as happened in Veneto region [8].

Both mercury and PFAS attempt at human and animal health. Therefore, developing effective remediation techniques is essential to achieve the 2030 Agenda Sustainable Development Goals.

1.2. Mercury

Mercury is a pollutant of global concern due to its toxicity and long-range transport in the atmosphere. The United Nations Environment Programme (UNEP) has classified mercury as a chemical toxic element to living organism. [9]

Mercury exists in various forms: inorganic mercury, including metallic mercury and mercurous and mercuric salts, and organic mercury, which includes compounds in which mercury is bonded to a structure containing carbon atoms. The organic forms are more dangerous than the inorganic ones, specifically methylmercury or ethylmercury [10] [11].

The human exposure can happen through inhalation, ingestion or skin contact. Elemental mercury vapor, often found in industrial settings or from broken thermometers, can be inhaled and absorbed through the lungs. Inorganic mercury compounds, sometimes used in cosmetics or traditional medicines, can be absorbed through the skin or ingested. At low levels, exposure to mercury causes gastrointestinal disturbances and weakness. On the other hand, at excessive levels, mercury damages the kidneys, immunological system, brain, muscles and ultimately leads to death. [10] [11]

Due to its natural presence on Earth, mercury can be released into the atmosphere through natural processes such as volcano eruptions and geothermal activity, or through human activities like fuel combustion and mining, as shown in Figure 2. [4]

Mercury emissions can be classified into primary and secondary emissions. When mercury is emitted in the environment for the first time from both anthropogenic and natural sources is defined as primary emissions. Conversely, secondary emissions, or mercury re-emissions, refer to the release of mercury, that has been stored in soils, sediments, or biomass, back into the environment, where it can be transported to new location. It occurs when mercury re-enters the air or water after having been previously removed. Approximately 10% of annual mercury emissions to the environment come from natural sources, with the remaining 30% coming from human activity. The re-emissions account for the remaining 60%. [4] [6]

Figure 2: Sources of mercury

As a part of global mercury cycle, mercury travels around the world through air, water and sediments with processes such oxidation, reduction, volatilization, settling, and photodegradation for up to 3,000 years after its release [6]. Therefore, mercury's point of emission has a global effect, not a local one. This means that even if in Europe mercury emissions have drastically decreased [12], it doesn't matter because mercury emissions have grown in developing nations like China and India.

Delving deeper into biogeochemical mercury cycle, mercury is released in the atmosphere by natural or anthropogenic sources (Figure 3) Figure 3: Mercury cycle . Once the mercury is released in the atmosphere, it can deposit on land and aquatic system and then revolatilized. Because of the anthropogenic activities such as mining, coal burning and industrial operations, mercury of long-term sedimentary storage has been released, thereby alternating the biogeochemical cycle. Therefore, higher mercury levels will continue to cycle among the atmosphere, ocean and land for centuries and millennials, unless an effective and rapid removal technology is developed. [13]

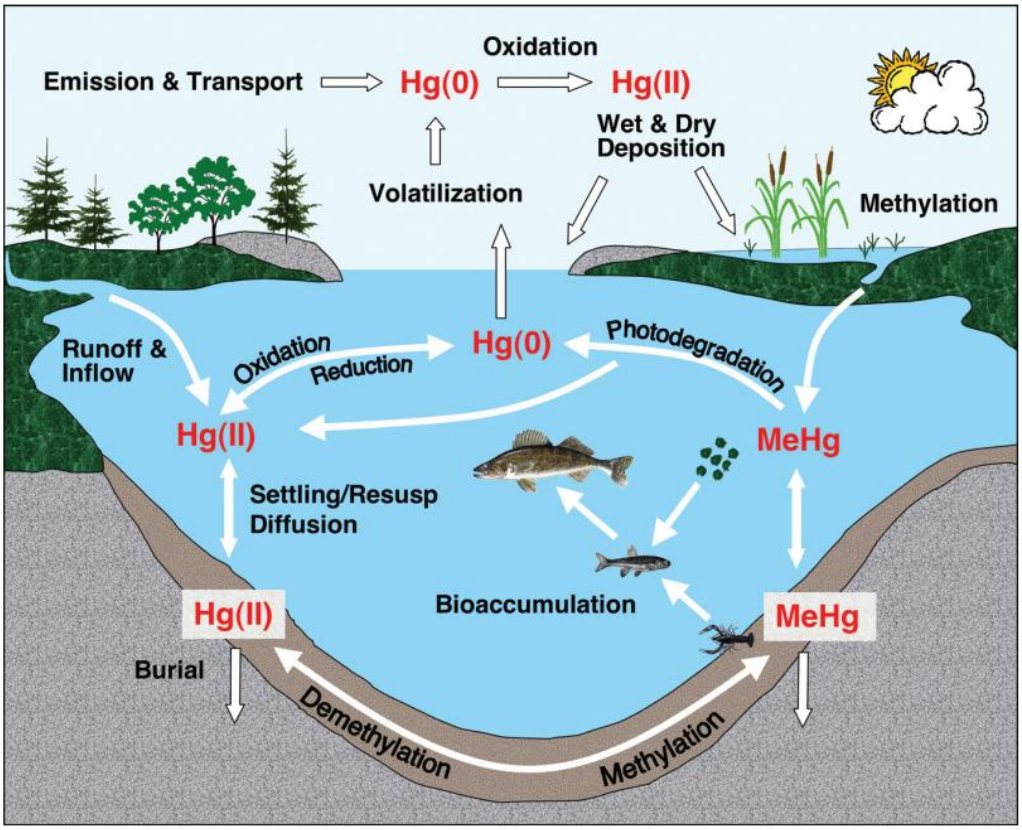

Figure 3: Mercury cycle [13]

In aquatic system, Hg^{2+} can be converted into dangerous methylmercury (MeHg) via microbial methylation, particularly in sediments. Methylmercury penetrates the food chain, building up in aquatic species. Frequently, the concentration of mercury in fish exceeds the standard set by the EU. Consequently, eating fish results in a serious health risk.

Two primary factors increase the quantity of mercury in aquatic animals: bioaccumulation and biomagnification (Figure 4). Bioaccumulation defines the accumulation of contaminants in an organism over time as a result of both environmental exposure and food consumption. Biomagnification refers to the increase of the concentration of mercury in animals from prey to predators through food webs [9]. Consequently, consuming fish and seafood contaminated with

methylmercury (MeHg) is the main and most dangerous route for humans to be exposed to mercury.

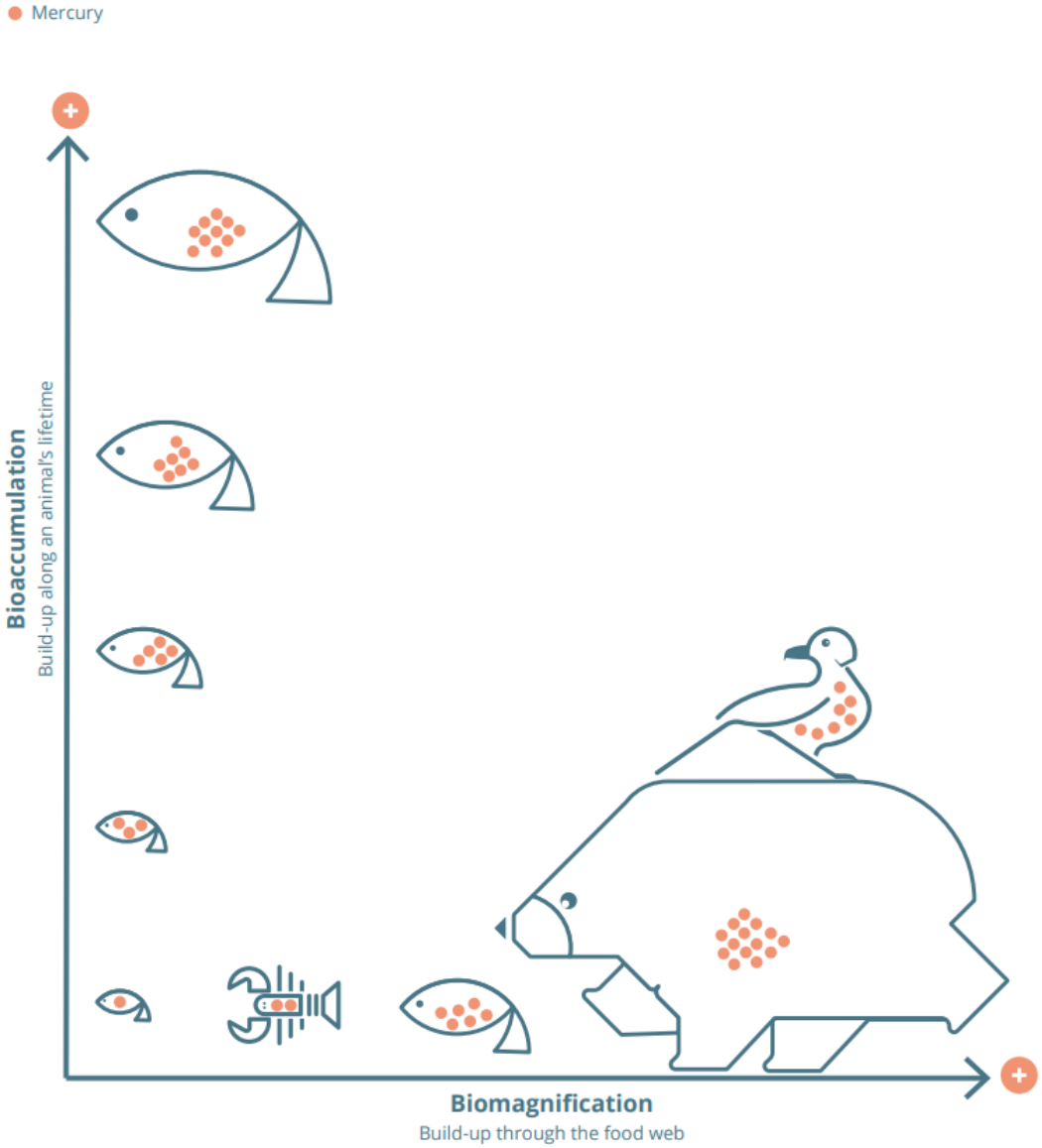

Figure 4: Bioaccumulation and biomagnification inside the food chain

Moreover, methylmercury can also be found in rice as well as in fish. Rice paddies are hot spots for mercury methylation and rice plants are efficient accumulators of MeHg. Due to the dissolution of mercury into water, it is very probable to cultivate rice with polluted water. [14]

To reduce and limit mercury concentration in the environment, effective remediation techniques have been developed. The major objective is to recover, reduce and reuse the existing mercury in the environment, separating it from contaminated media or transforming it into less toxic species [15] [16] [17] [18] [19] [20].

Conventional methods include adsorption, thermal desorption, chemical oxidation/reduction, membrane filtration and precipitation. Adsorption is widely used due to its simplicity and low cost, while thermal and chemical treatments are effective but energy-intensive and can generate secondary waste.

Biological and electrochemical methods represent alternative remediation strategies. Electrokinetic remediation uses an electric field gradient to drive mercury ions towards electrodes for extraction. However, the process requires continuous power supply and specialized electrode materials, resulting in relatively high operational costs. Phytoremediation and microbial remediation rely on plants and microorganisms, respectively, to remove, degrade or stabilize pollutants. Their main limitations are the slow removal rate and the strongly dependence on the environment conditions.

Emerging materials such as nanomaterials and metal organic frameworks (MOFs) provide high adsorption capacity and selectivity for mercury, aiming to be inexpensive reusable and environmentally friendly. Despite promising performance, challenges related to stability, scalability and cost remain. [15] [18] [20] [21]

Overall, mercury remediation technology continues to evolve, with adsorption and bioremediation emerging as promising techniques, focusing on feasibility and sustainability. However, research must be focused on developing remediation procedures that are more durable and sustainable, reducing both toxic residues and the entire environmental impact of remediation.

1.3. Per- and Poly- Fluoroalkyl Substances: emerging contaminants

Per- and Poly- Fluoroalkyl Substances (PFAS) indicates a large group of man-made chemicals. PFAS have an aliphatic carbon chain in which fluorine molecules have replaced the hydrogen partially or completely [7].

PFAS are one of the most common synthetic emerging chemicals, initially introduced in the 1940s and now frequently used in a variety of industrial products such as firefighting foams and food packaging [22]. But not only, PFAS have been considerably used in the pesticide formulation, firefighting foams, aerospace aviation, automotive, oil production and many other industrial products [23]. Their non-stick, water-repellent and high temperature stability properties make them difficult to replace despite concerns about human exposure and environmental persistence. [24]

As a result of this extreme persistence, PFAS are commonly referred to as “forever chemicals” [23] [25]. Their persistence primarily arises from their highly stable molecular structure. In particular, the carbon–fluorine bond confers exceptional thermal and chemical stability, making these compounds resistant to physical, chemical, and biological degradation.

PFAS include a large and diverse group of compounds and therefore, can be classified according to their chain length. Long-chain PFAS are classified as a perfluoroalkyl chain with seven or more carbon atoms whereas short-chain PFAS contain less than seven carbon atoms. Another classification is based on their polymeric nature, due to the very different chemical, physical and biological properties that distinguish polymeric and non-polymeric form. [26]

While thousands of different PFAS exist, only a few are being tracked and have regulatory problems, such as perfluorooctanoic acid (PFOA) [27]. PFOA is one the most commonly identified and frequently detected in the global environment and especially in European wastewaters. [7] Its chemical structure is illustrated in Figure 5.

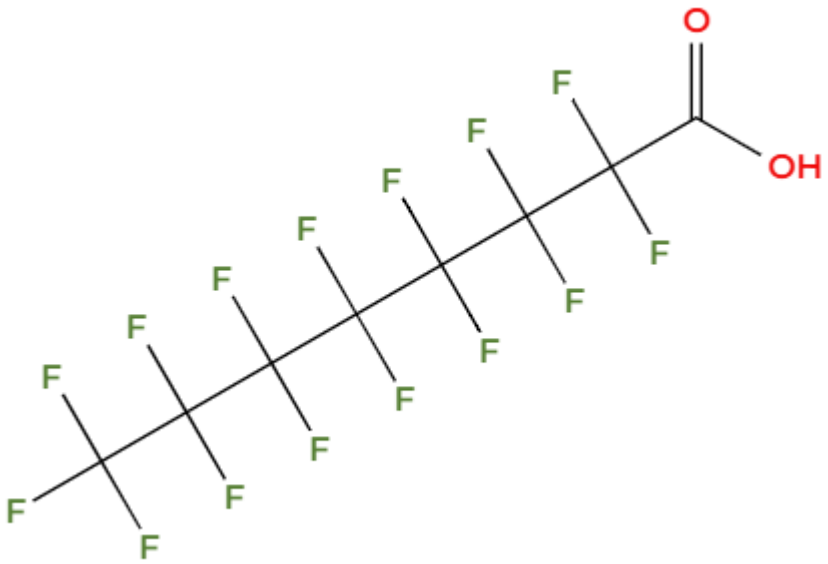

Figure 5: Structure of perfluorooctanoic acid (PFOA)

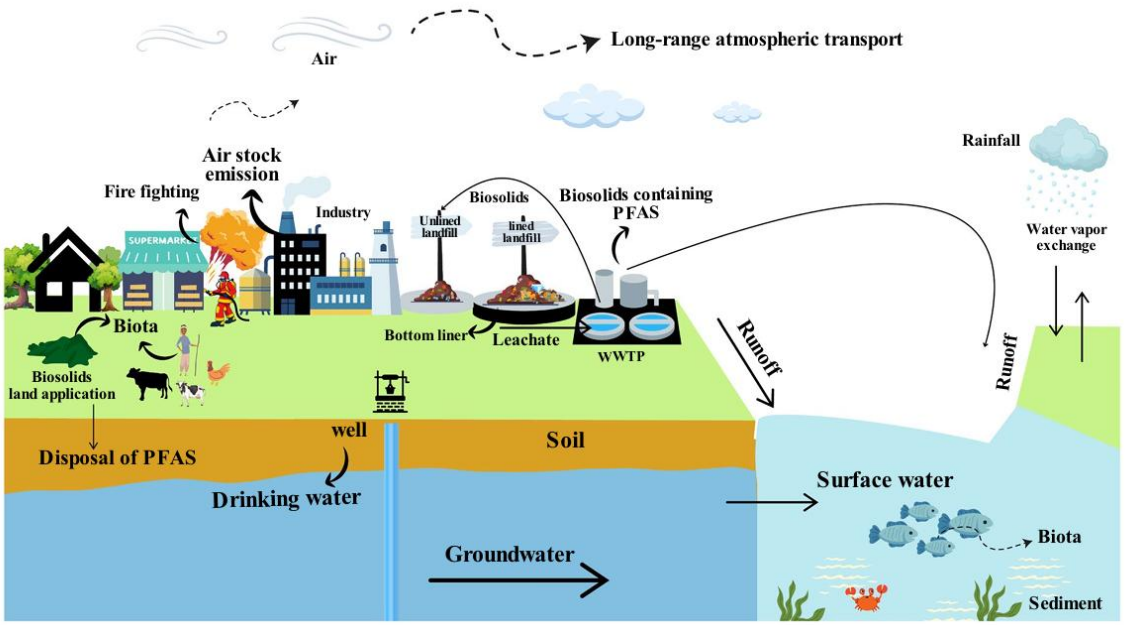

Figure 6: Routes, fate and mechanism pathways of PFAS in different environmental matrices [25]

PFAS emissions can be categorized into direct and indirect sources. Direct sources are emissions from PFAS-containing products, industrial activities and solid waste disposal while indirect sources include atmospheric deposition and runoff [25]. However, due to the chemical stability and mobility properties, once PFAS are emitted in the environment, they can travel and migrate in the atmosphere, soil, water, as shown in Figure 6. Atmospheric transportation and run off play an important role in spreading PFAS around remote areas and aquatic environment [24]. Consequently, the point of emission is irrelevant. Indeed, PFAS has been found in the most remote and rural areas on the globe [28]. Moreover, in their anionic forms, which are water-soluble, they can migrate from soil to groundwater and be transported at long distance [8].

The persistence and bioaccumulation properties of PFAS and their potential to travel across different media is one of the main concerns. PFAS affect all types of environments, water resources, sea, drinking water, soils. PFAS bioaccumulate in living organisms due to their hydrophobic, lipophobic, heat-resistant, and non-biodegradable properties. [24]

The human exposure (Figure 7) mainly happens by ingestion of contaminated water, food or inhalation of dust [8]. Their effects (Figure 7) depend on the exposure's condition such as magnitude, duration and factors associated with the individual, including age, sex, health [29]. Some studies [23] [29] [30] [31] have shown that PFAS alter human development, lipid metabolism, endocrine system, immunotoxicity, hepatotoxicity and reprotoxicity. PFOA and PFOS are the most frequently compound

detected in human serum and in particular, PFOA has been classified has cancerogenic. [32]

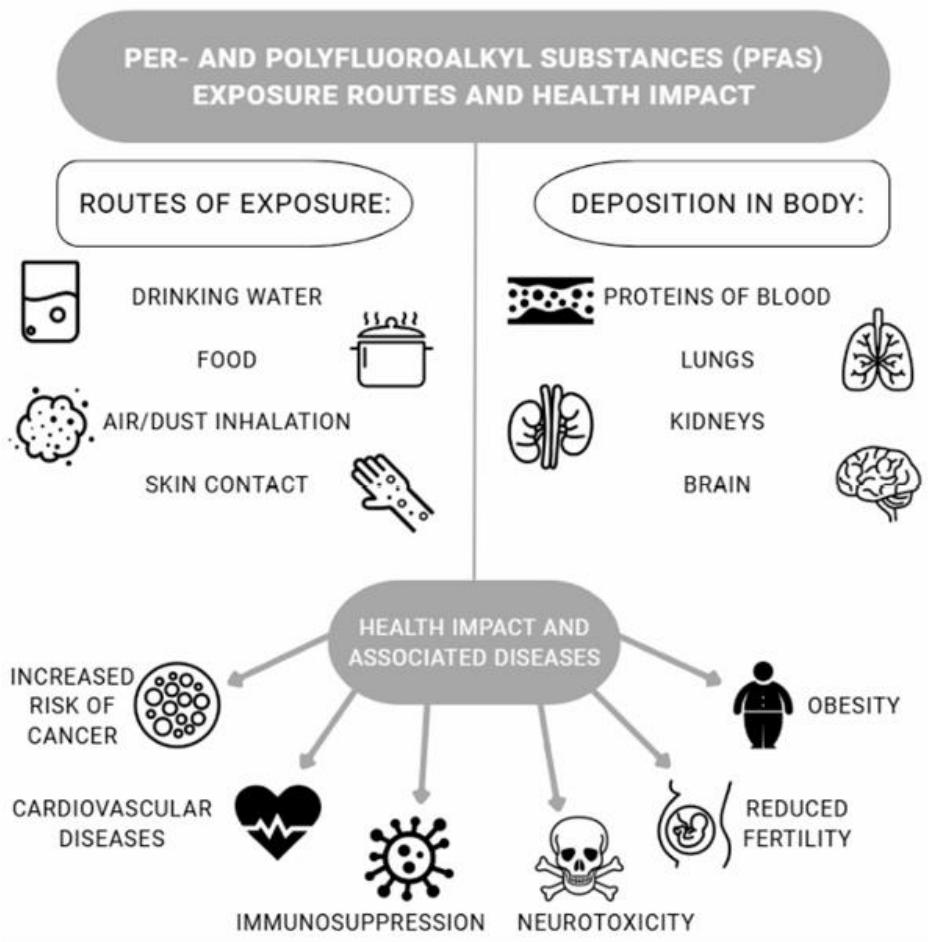

Figure 7: Routes of PFAS exposure and their potential health effects [24]

Due to high risks of PFAS exposure, treatment methods have been designed. The techniques can be divided into separation and destructive. [7] [23] [28] [33] [34]

Separation methods are based on the removal of PFAS from a medium using chemical processes, without altering the chemistry. The most separation methods used are adsorption with activated carbon, ion exchange resins, membrane filtration, soil excavation. However, these techniques need further treatment and disposal of contaminated material.

In contrast, destructive methods are based on the destruction of PFAS chemical structure by chemical or thermodynamic processes, transforming them into less harmful chemicals. The most destructive methods used are thermal treatment, electrochemical oxidation, ultrasound, biological methods. While effective, these methods are energy-intensive and often difficult to scale.

1.4. Cellulose as sustainable material for adsorption

Due to global challenges, such as climate change and depletion of fossil resources, there is growing interest in bio-based products. Cellulose is the most abundant, renewable, and biodegradable biopolymer present on Earth, giving it an environmentally friendly alternative. It is produced in large quantities each year and decomposes spontaneously in a completely sustainable, carbon-neutral process. [35]

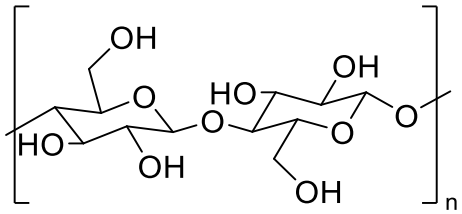

Figure 8: Cellulose structure

Cellulose is a linear macromolecule formed by β-1,4-linked-D-glucopyranose rings. The chemical structure is shown in Figure 8. It is colourless, odourless, tasteless, non-toxic and exhibits intriguing properties such as excellent mechanical strength, biocompatibility, hydrophilicity, relative thermal-stability, high sorption capacity, and alterable optical appearance. The bond between the units is made through condensation of the hydroxyl groups present on the monomer, forming chains with high tensile strength. The single polymer chains assemble into fibers through intermolecular hydrogen bonds and hydrophobic interactions. Cellulose is insoluble in water due to its crystalline structure and intramolecular and intermolecular hydrogen bonds. [35] [36]

Nanocellulose is defined as a cellulosic material with at least one nano-sized dimension. It has all the properties of cellulose such as high biodegradability and high mechanical strength, adding an incredibly versatility and high surface area. Moreover, it is possible to create a cellulose-based nanomaterial with excellent adsorbent properties, making it particularly suitable for remediation.

There are multiple forms, which are defined by their morphology and source: cellulose nanocrystals (CNC), cellulose nanofibers (CNF) and bacterial nanocellulose (BNC). CNC and CNF are mainly produced in a top-down approach, with bulk plant material gradually broken down into nanoscale structures using chemical, mechanical, or enzymatic treatments. Cellulose nanocrystals are stiff, rod-like crystalline particles with high crystallinity (54-88%) obtained by extensively removing amorphous regions. They are most typically made using strong acid hydrolysis, specifically sulfuric acid. In contrast, CNF are composed up of long, flexible, and highly fibrillated cellulose fibers with significant amorphous content, with widths ranging from tens to several hundred nanometres and lengths in the micrometre range; mechanical treatments such as high-pressure homogenization, cryo-crushing, and grinding are commonly used for their extraction. Distinct from plant-derived nanocelluloses, BNC is produced directly

by Gluconacetobacter xylinus in nutrient-rich aqueous conditions, resulting in very pure cellulose without the need for substantial pretreatment. All of them exhibit high mechanical strength, transparency and are chemically reactive. However, the properties of nanocellulose significantly depend on their production technique, the cellulose source and their final application. [37] [38]

Cellulose is highly reactive due to its hydroxyl groups, allowing for chemical modification. Surface modification of nanomaterial is crucial in enhancing their properties for specific application. By tailoring the surface characteristics, nanocellulose can achieve enhanced electrical conductivity, mechanical strength and hydrophobicity [37] [39]. The possible functionalizations are reported in Figure 9, which also shows other related functional groups such as oxidation, esterification, amidation.

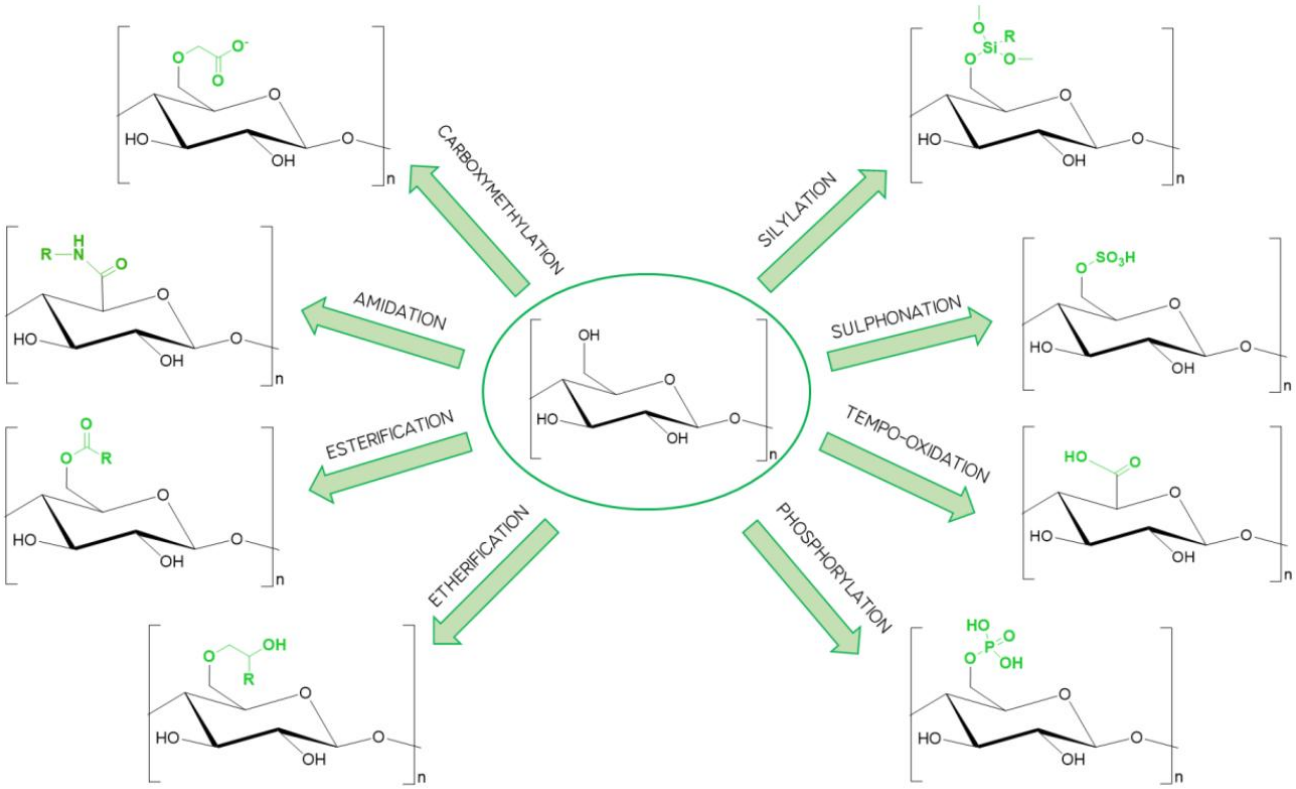

Figure 9: Cellulose functionalization reactions at C6 position [36]

Cellulose nanofibers can be used as building blocks, in combination with crosslinkers, to synthesize three-dimensional porous material. [36] [40]

A xerogel made of TEMPO-oxidized cellulose nanofibers and bPEI has shown high efficacy in removing dyes and heavy metals from wastewater. The carboxyl groups, produced by TEMPO-mediated oxidation, considerably increase heavy-metal adsorption capacity by offering a large number of negatively charged binding sites. The addition of bPEI, a polymer with ethylenediamine repeating units, improves the material's performance. Its amino groups enhance significant interactions with

pollutants via chelation, boosting the total affinity for both heavy metals and organic toxins [36] [40].

Similarly, Ateia *et al*. investigate the adsorption capacity of PEI-functionalized cellulose nanocrystals for PFAS removal. The material demonstrated near-instant adsorption equilibrium, achieving high removal efficiency for 22 different PFAS compounds [41].

In conclusion, PEI-functionalized cellulose exhibits high adsorption capacity for both mercury and PFAS. This highlights the strong potential of modified cellulose-based materials as efficient and sustainable alternatives for water remediation.

1.5. State of the art and research perspectives

1.5.1. Treatment of marine sediments and scale-up of CNS production

Marine sediments tend to accumulate contaminants, acting both as a sink and a secondary source of pollution. Their high organic content enhances the contaminant adsorption, facilitating the movement of pollutants through water and its entrance in the food chain [42]. Among all contaminants, mercury and PFAS are frequently detected in marine sediments [43] [44]. Both pollutants are highly toxic and exhibit a strong tendency to bioaccumulate within aquatic ecosystems.

Sediment remediation is particularly challenging due to the risk of resuspension and the subsequent release of contaminants [45]. Consequently, in-situ sediment capping is becoming the predominant remediation technique. It consists of physically isolate contaminated sediments, reducing contaminant mobility and preventing pollutants resuspension. Materials with high porosity and high surface areas, such as activated carbon and biochar, are commonly used as capping materials. [42] [44]

Nanocellulose represents a promising capping material due to its high surface area, mechanical strength, environmental compatibility and, additionally, can be chemically functionalized.

Despite the exceptional qualities of cellulose, the quantity needed to perform a sediment capping is extremely high. Therefore, optimizing large-scale nanocellulose production is essential. In particular, scaling up the production of TEMPO-oxidized nanocellulose is a challenging task that necessitates the integration of energy-efficient mechanical fibrillation, precisely controlled oxidation chemistry, and continuous process control within a modular, safe, and chemically optimized industrial plant.

1.5.2. Optical analysis and porphyrins

Heavy metals, in particular mercury, are widely known for their severe harmful impacts on ecosystems and human health. Their uncontrolled discharge into water sources and subsequent presence in drinking water constitute a huge global concern

[11]. Consequently, there is an urgent need for cost-effective, accessible, and efficient technologies to detect these pollutants at very low concentrations. [46]

Traditional methods for Hg^{2+} detection, including atomic absorption spectroscopy (AAS), atomic fluorescence spectrometry (AFS), and inductively coupled plasma mass spectrometry (ICP-MS), have been widely employed due to their high sensitivity and reliability. However, these procedures necessitate expensive devices and complex sample preparation, limiting their use for rapid, on-site, and real-time analysis. Recently, a variety of innovative approaches for detecting Hg^{2+} by colour change have been developed that do not require the use of special equipment [47]. In this context, optical sensors have emerged as a promising solution due to the simplicity of use, sensitivity, and suitability for real-time monitoring. Moreover, commonly used electronic devices like webcams and smartphones can be used to generate economical sensing platforms, making optical sensors readily accessible for real-world uses [48] [49].

Over the past decade, several receptors have been reported in the literature for the colorimetric and fluorometric detection of heavy metal ions. Among these, porphyrins have been chosen as sensing material in this work because of the richness of their photophysical properties and the possibility to tune them by synthetic modification [50]. Porphyrins are naturally occurring macrocyclic compounds containing four pyrroles connected in macrocyclic fashion through four methine carbons at their α-positions. Porphyrin-based chemosensors have demonstrated considerable success in the selective detection of a wide range of metal ions [51].

In the research of Liu *et al.* [47], the porphyrin-functionalized fibre exhibited an immediate and distinct colour change from red-brown to dark green upon immersion in a Hg^{2+} solution. This clear and rapid visual response indicates excellent selectivity toward Hg^{2+}, enabling simple, real-time, on-site detection by the naked eye. The competition experiments demonstrate that the fibre sensor has predominant selectivity to Hg^{2+} and strong capability against the existence of the other interference metal ions.

The promising work carried out by the Sensor Group at the University of Rome "Tor Vergata" is a significant application of porphyrin-based chemosensors. In this study conducted by Caroleo *et al*. [46], the porphyrin compound was placed onto an affordable and easily available solid substrate, specifically a Colour Catcher sheet. As seen in Figure 10, the substrate clearly changed colour from dark pink to dark green when mercury ions were present. Furthermore, the suggested sensing device showed exceptional sensitivity, detecting traces of mercury ions in aqueous samples down to 10^{-1} M with a very quick reaction time.

Figure 10: Colorimetric variation of CC@TTPCH$_2$ caused by the mercury coordination [46]

Additionally, this method was evaluated using porphyrins sensitive to fluoride ions. [52]. The results demonstrated excellent reproducibility, high sensitivity, and a rapid response time. As shown in Figure 11, the substate changes colour from pink to dark green when exposed to fluorine ions.

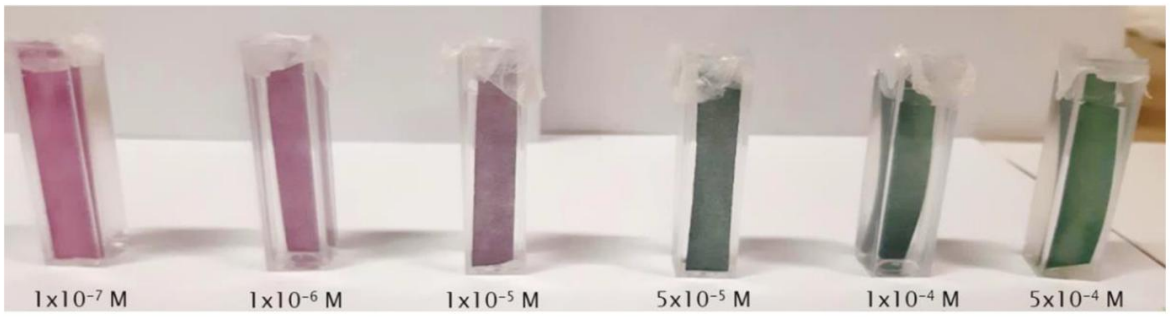

Figure 11: Colorimetric variation of CC@SiTTC caused by fluorine ions [52]

Coupled with the system's compact and portable design, this approach is ideally suited for real-time, on-site monitoring of natural water sources, enabling efficient detection of contaminants even in complex environmental matrices."

1.6. Aim of the Thesis

The aim of this thesis is to develop and optimize a cellulose-based nanostructured xerogel able of simultaneously detect and adsorb aquatic contaminants, in particular mercury and PFAS. This research is a carried out through a collaboration between the *Organic Synthesis Catalysis and Materials Laboratory* 'O^{SCM} Lab' of Politecnico di Milano and the *Sensor Group* at the University of Rome – Tor Vergata.

Cellulose-based nanostructured materials represent promising candidates for water remediation due to their renewability, biodegradability, environmental sustainability, high surface area, and ease of chemical functionalization. These features enable cellulose to act as an efficient adsorption platform for a wide range of contaminants.

To integrate detection capabilities, the nanostructured xerogels were functionalized with porphyrinic moieties. Porphyrins were selected as sensing elements owing to their remarkable photophysical properties, high sensitivity toward metal ions, and the possibility of structural tuning through synthetic modification. The coexistence of adsorption and sensing functionalities allows the material not only to remove contaminants from water but also to monitor pollutant uptake in real time until saturation. In particular, the colorimetric response of the porphyrinic sensors, correlated with the amount of adsorbed contaminants, enables naked-eye detection.

This work investigates different functionalization strategies to optimize both adsorption efficiency and sensing performance, while evaluating the morphological and chemical properties of the developed materials through advanced characterization techniques.

Furthermore, since significant mercury adsorption was observed also for pristine nanosponges, the potential application of cellulose-based materials as capping agents for the remediation of contaminated marine sediments was considered. In view of the large material volumes required for such environmental applications, a preliminary evaluation of the scalability of the synthesis process was also conducted to assess the feasibility of large-scale production.

2 Methods and Materials

2.1. Production of materials

Reagents were purchased from Merck KgaA (Darmstadt, Germany). Cotton linters (99% purity) was provided by Bartoli Spa paper mill (Capannori, Italy).

Deionized water was produced with Millipore Elix® Deionizer with Progard® S2 ion exchange resins. Other instruments used include a magnetic stirrer, Fisher™ Model 505 Sonic Dismembrator with a 13 mm probe tip, SP Scientific BenchTop Pro Lyophilizer, Thermo scientific Sorvall ST 8 Centrifuge, Argo LAB TCF50 oven, Biotage Microwave reactor, a Hanna Instruments HI522–02 pH-meter and conductometer.

2.1.1. Production of porphyrinic molecules

The Sensor Group at the University of Rome "Tor Vergata" provided the porphyrinic molecules, which they synthesized following the procedures outlined below.

2.1.1.1. Production of 5,10,15,20-tetrakis(4-carboxyphenyl) porphyrin ($TTPCH_2$)

The synthesis of 5,10,15,20-tetrakis(4-(methoxycarbonyl)phenyl)porphyrin is illustrated in Figure 12 and proceeds through two steps [52]:

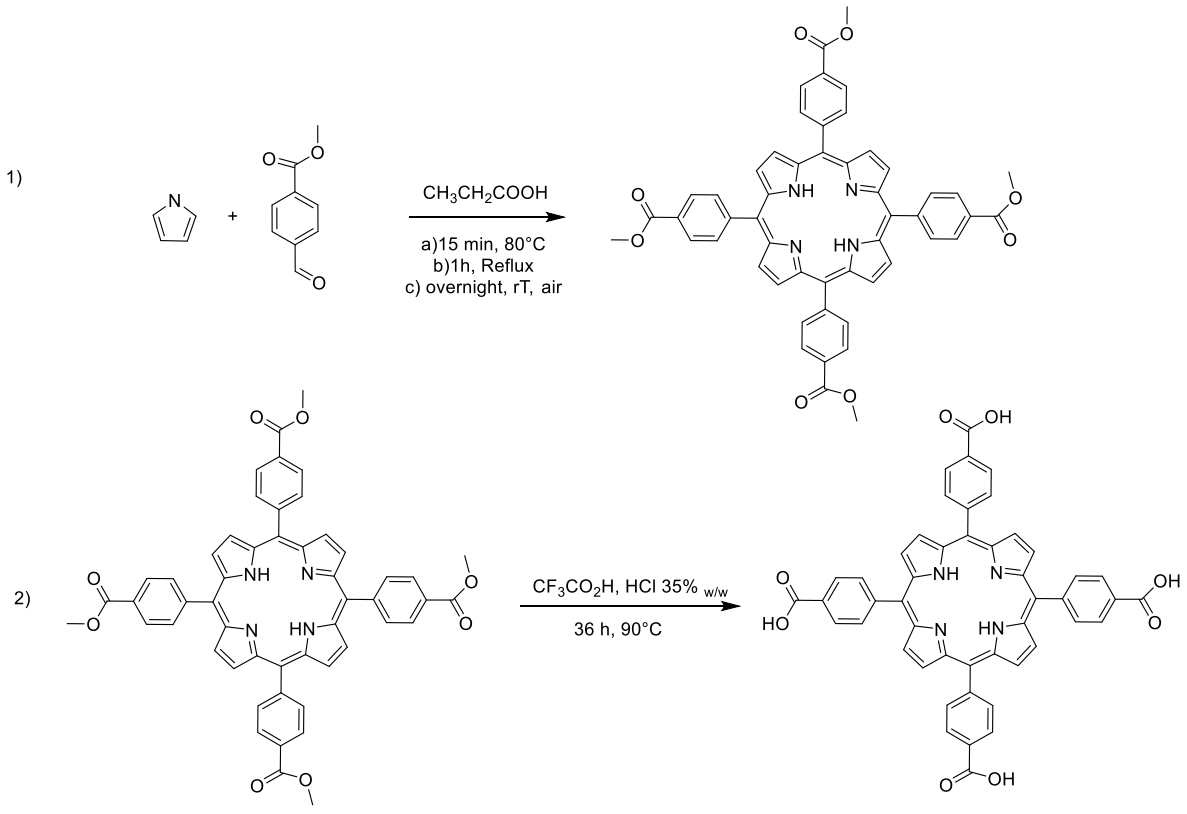

Figure 12: synthesis of 5,10,15,20-tetrakis(4-(methoxycarbonyl)phenyl)porphyrin

1. Preparation of 5,10,15,20-tetrakis(4-(methoxycarbonyl)phenyl)porphyrin was performed using the Adler Longo procedure with some changes [53]. In a 1 L round-bottom flask, p-methoxycarbonyl benzaldehyde (1.312 g, 8.0 mmol) was added to 100 mL of propionic acid. The solution was stirred at 80 ◦C. In a separate flask, a propionic acid solution (20 mL) of freshly distilled pyrrole (0.56 mL, 8.0 mmol) was added dropwise to the previous solution for at least 15 minutes. Then the solution was refluxed for 1 hour. The reaction mixture was cooled and allowed to stand overnight under air atmosphere. After filtering, the solid product was washed several times with hot water and methanol (1:9) solution in order to remove unreacted propionic acid and impurities. Then the resulting black purple powder was vacuum dried and separated by thin layer chromatography with silica gel-coated glass plates using a mixture of dichloromethane–hexane (5:1) as eluent. Product was purple crystals with 41 % yield. ^{1}H-NMR (700 MHz, $CDCl_3$) δ (ppm): 8.45 (8H, d, J=7.25 Hz, Ar-meta- H), 8.82 (8H, s, β-H), 8.29 (8H, d, J=7.25 Hz, Ar-orto-H), 4.11 (12H, s, CO_2CH_3), 2.79 [2H, s, NH].
2. 5,10,15,20-tetrakis(4 -(methoxycarbonyl)phenyl)porphyrin (0.100 g, 0.12 mmol) was dissolved in CF_3CO_2H (5.0 mL) and aqueous HCl solution (35 %; 2.5 mL) and then heated at 80–90 ◦C for 36 h. The reaction mixture was extracted with ethylacetate and water. The organic layer was evaporated to produce 5,10,15,20-tetrakis(4-carboxyphenyl) porphyrin (H_2TCPP). ^{1}H-NMR (700 MHz, DMSO-d_6): δ (ppm) = 13.37 (4H,s, COOH), 8.77 (8H, s,β-H), 8.31 (8H, d, J=8 Hz, Ar-meta-H), 8.23 (8H, d, J=8 Hz, Ar-orto-H), 2.99 [2H, s, NH].

2.1.1.2. Production of tetra(4-sulfonatophenyl)porphyrin ($\boldsymbol{TPPS_4}$)

The synthesis of tetra(4-sulfonatophenyl)porphyrin is illustrated in the Figure 13 and proceeds through two steps following a procedure reported in literature [54]:

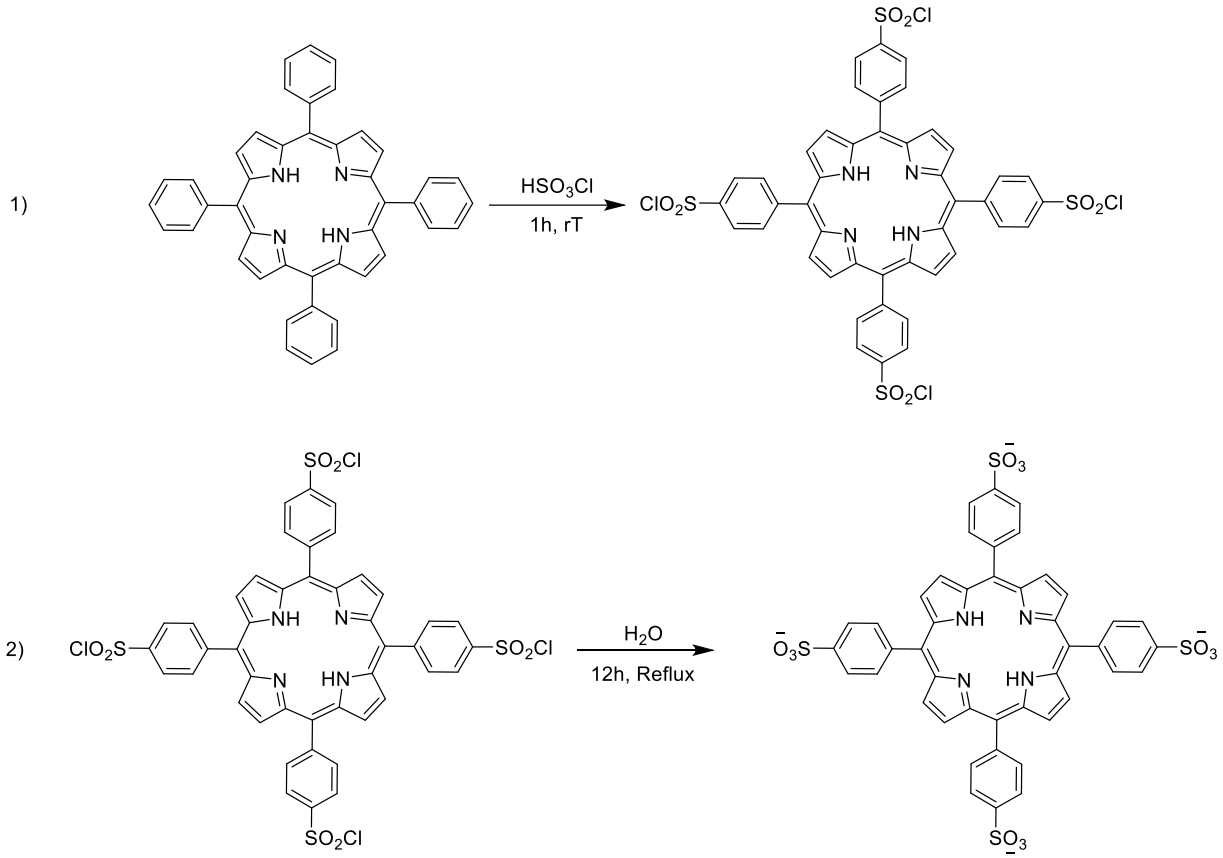

Figure 13: Synthesis of tetra(4-sulfonatophenyl)porphyrin

1) Chlorosulphonation; 5,10,15,20-Tetrakisphenylporphyrin (100 mg, 0.162 mmol) and chlorosulphonic acid (6 ml, 90 mmol) were stirred at room temperature for 1 h. To the resulting solution was added slowly and carefully, 40 g of ground ice to give a green crystalline precipitate of deprotonated 5,10,15,20-tetra(4-chlorosulphonylphenyl)porphyrin. After addition of the ice, 30 ml of distilled water was added and the free base was liberated from this mixture through the gradual addition, with stirring, of a slight excess of saturated aqueous $NaHCO_3$. When neutralization was complete, the solution changed from a bright green to a dark red final of the neutral form. The required compound was extracted immediately into $CHCl_3$, which was then dried (Na_2SO_4) and evaporated to give the solid 5,10,15,20-tetra (4-chlorosulphonylphenyl)porphyrin. (120 mg, 73%). λ_{max} ($CHCl_3$): 418 nm, 516 nm, 554 nm, 590 nm, 650 nm. ^{1}H-NMR ($CDCl_3$), δ (ppm): 8.90 (8H, s), 8.20 (8H, d, J = 7.5 Hz), 7.50 (8H, d, J = 7.5 Hz), -2.70(2H, s). The chlorosulphonyl compound is usually obtained in pure form by this process. If further purification is required, the crude product can be purified by chromatography on silica gel using $CHCl_3$ as the eluent.

2) Hydrolysis of Chlorosulphonyl product: a suspension of 5,10,15,20-tetra(4-chlorosulphonylphenyl)porphyrin (70 mg, 69 mmol) in water (120 ml) was refluxed for 12 h. The resulting solution was concentrated by rotary evaporation to give the required 5,10,15,20-tetra(4-sulfonatophenyl)porphyrin which was further purified by passage through a Sephadex column (G25), using water as eluant. A purple-orange

band was eluted, and all fractions were collected, the mixture H_2O/Acetone lead to the precipitation of the final required solid 5,10,15,20-tetra(4-sulfonatophenyl)porphyrin (58 mg, 90%). λ_{max} (H_2O): 418 nm, 512 nm, 548 nm, 594 nm, ^{1}H-NMR (D_2O), δ (ppm): 8.75 (8H, s), 8.30 (8H, d, J = 7.7 Hz), 7.20 (8H, d, J = 7.7 Hz).

2.1.1.3. Synthesis of (Hydroxy)[5,10,15-tritolycorrolato]silicon, (SiTTC)

The (Hydroxy)[5,10,15-tritolycorrolato]silicon (SiTTC) was prepared according to the procedure present in literature [55], illustrated in Figure 14.

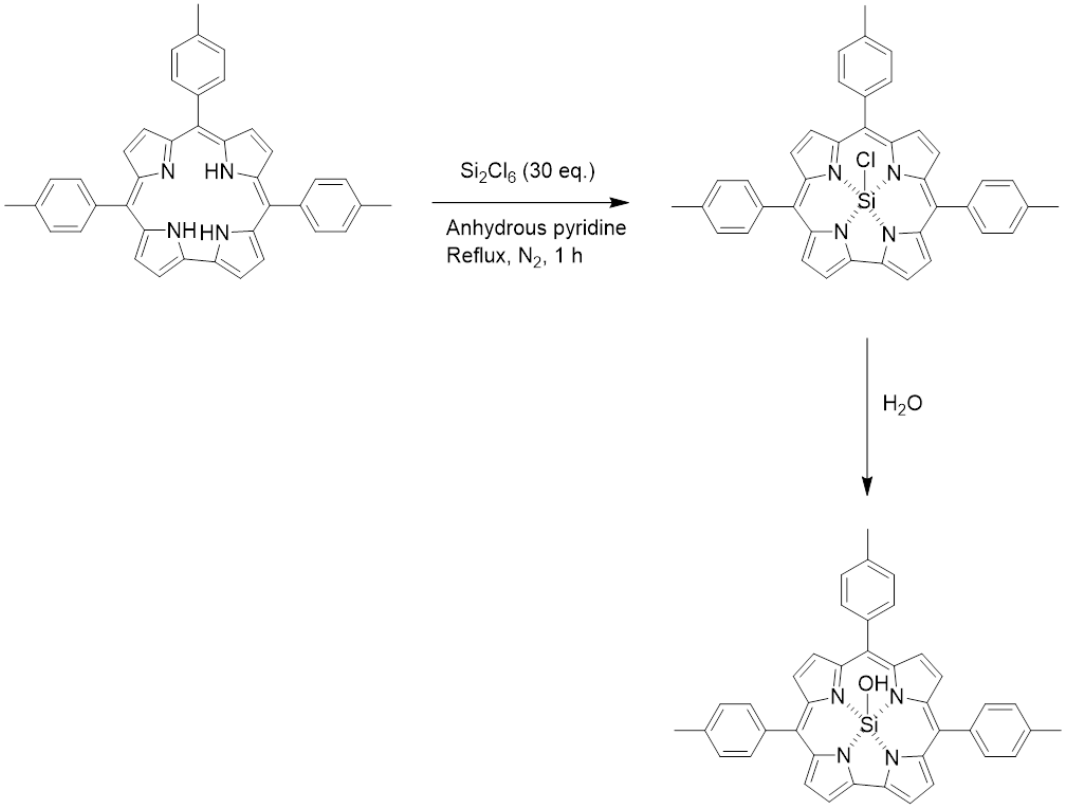

Figure 14: Synthesis of (Hydroxy)[5,10,15-tritolycorrolato]silicon

5,10,15-Tritolylcorrole free base $TTCorrH_3$ (60 mg, 0.106 mmol) was dissolved in anhydrous pyridine (20 mL) and the mixture heated under nitrogen. Si_2Cl_6 (547 mL, 3.18 mmol, 30 equivalent) was added under inert atmosphere and the mixture was further stirred under reflux for 1h The solution became dark green then pink. Once complex formation was verified by UV/Vis spectroscopy, the mixture was left to cool and then quenched by careful addition of water. The residue was filtered on paper to remove the silica formed and immediately dissolved in methanol/THF (1:1). Solvent was removed and the residue purified by column chromatography on Al_2O_3 by eluting with CH_2Cl_2 to collect the μ-oxo dimer, and then with $CHCl_3$ for SiTTC.

(Hydroxy)[5,10,15-tritolylcorrolato]silicon SiTTC: Crystallized from CH_2Cl_2/methanol. Yield: 45mg (70%). M.p. >300°C. UV/Vis (CH_2Cl_2; λ_{max} [nm] (lg ε [$M^{-1}cm^{-1}$]): 389 (4.75), 409 (5.54), 519 (4.00), 532 (4.01), 559 (4.30), 578 (4.52); ^{1}H NMR (400.13 MHz, $CDCl_3$): δ=

9.36 (d, 2H, J=4.26 Hz, β-pyrrole), 9.20 (d, 2H, J=4.87 Hz, β-pyrrole), 9.07 (d, 2H, J=4.29, Hz, β-pyrrole), 8.90 (d, 2H, J=4.88, Hz, β-pyrrole), 8.18 (unresolved multiplet, 5H, *meso*-phenyl), 7.92 (d, 1H, J=7.63 Hz, *meso*-phenyl), 7.61 (m, 5H, *meso*-phenyl), 7.54 (d, 1H, J=7.69 Hz, *meso*-phenyl), 2.70 (s, 6H, phenyl-CH_3), 2.69 (s, 3H, phenyl-CH_3), -4.46 ppm (br s, 1H, SiOH); MS (FAB): *m*/*z* 747 [M-OH + nitrobenzyl alcohol)] (100%) ; elemental analysis (%) calcd for $C_{40}H_{30}N_4OSi$:C 78.66, H 4.95, N 9.17; found: C 78.74, H 4.98, N 9.12.

2.1.2. Production of TEMPO-oxidized cellulose nanofibers

2.1.2.1. TEMPO-oxidation

Cellulose oxidation is conducted via a TEMPO-mediated catalytic system, following the procedure of Isogai et al. [56]. Virgin spruce cellulose is used as starting material and the oxidation system is based on TEMPO/KBr/NaClO system.

The catalytic system was obtained by dissolving 15.42 g of KBr and 2.149 g of 2,2,6,6-tetramethylpiperidine-1-oxyl radical (TEMPO) in 2 L of deionised water. Simultaneously, 100 g of cellulose was soaked in 3 L of deionized water and blended to obtain a homogeneous pulp. Once achieved homogeneity in both mixtures, the catalytic solution was added to the cellulose suspension to start the reaction system, illustrated in Figure 15.

The pH of the suspension was continuously monitored using a calibrated pH meter. A total of 440 mL of NaClO was added dropwise via a dropping funnel, while the pH was maintained above 10.5 to ensure the reaction outcome. The gradual decrease in pH during NaClO addition indicates the onset of the oxidation reaction, due to the gradual formation of carboxyl groups. Therefore, a 4 M NaOH solution was employed to counteract the pH drop and stabilize the system. Once the pH was stabilized, the reaction mixture was left to proceed under ambient conditions overnight. After 12–15 hours, the reaction was quenched by adding 37% HCl, lowering the pH to 2–3. To isolate the cellulose fibers, the reaction mixture was vacuum-filtered through a cotton filter and thoroughly washed with deionized water until the pH reaches neutrality, obtaining TEMPO-oxidized cellulose (TOC).

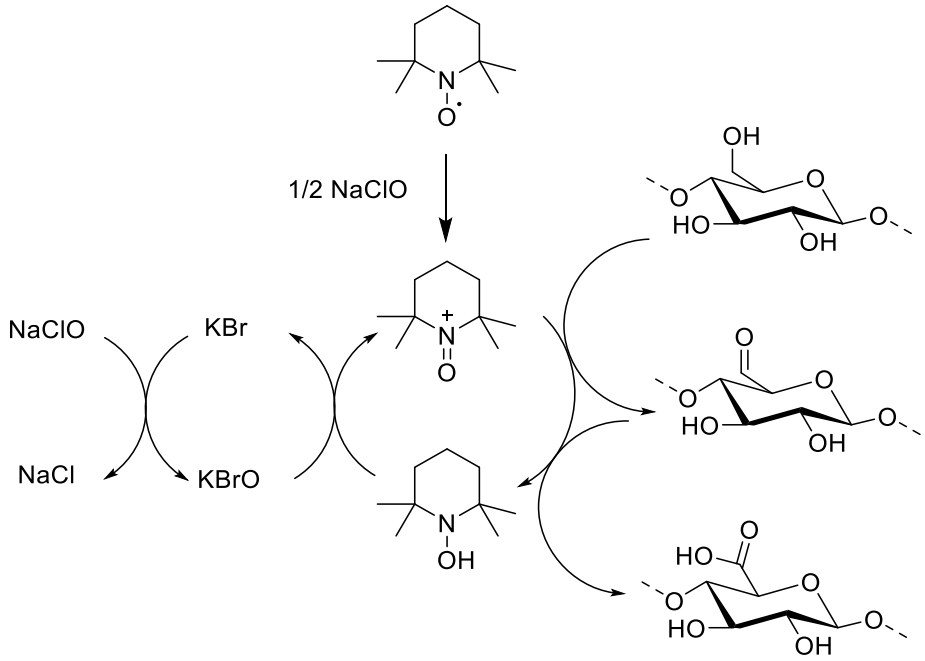

Figure 15: TEMPO-mediated oxidation of cellulose, showing TEMPO catalytic cycle

An alternative TEMPO-mediated oxidation method was tested, following the procedure described by Arfelis *et al.* [57].

To achieve an oxidation degree of 1.3-1.4 $mmol_{COOH}/g_{cell}$, , the following reagents were used for 1g of dry cellulose pulp: 10 mmol of sodium hypochlorite NaClO, 16 mg of 2,2,6,6-tetramethylpiperidine-1-oxyl radical (TEMPO) and 0.1g of sodium bromide NaBr. Deionized water was added to prepare a 1% (w/v) suspension.

First, cellulose was dispersed in distilled water containing TEMPO and NaBr and the mixture was stirred for 15 min to ensure homogeneity. Subsequently, 30 mL of NaClO was added to start the oxidation reaction. As the reaction proceeded and the pH dropped below 10, an additional 30 mL of NaClO was added. This stepwise addition continued until the total intended volume of NaClO was incorporated. Only after the complete addition of NaClO, the pH was maintained above 10 by the gradual addition of 0.5 M NaOH. Once the pH stabilized at 10, the reaction was considered complete.

The oxidized cellulose suspension was then vacuum-filtered and thoroughly washed with deionized water until the filtrate reached neutral pH, yielding TOC.

The oxidation results in the partial regioselective conversion of the primary alcoholic moieties at C6 position of the glucopyranose units into the corresponding carboxylic acids. The carboxyl content of TOC prepared *via* the two different aforementioned procedures was determined by conductometric titration, following the procedure of [58], [59]. Briefly, a well-defined quantity of TOC (50-100 mg) was dissolved in 15 mL of HCl 0.01M and the minimum volume of deionised water needed to allow efficient agitation. Once the TOC suspension had achieved homogeneity, the titration was

performed under continuous stirring. The titrant, sodium hydroxide NaOH 0.01 M, was added incrementally in 0.5 mL steps. After each addition, the electrical conductivity of the suspension was measured and recorded. The procedure continued until the conductivity values return to or exceed the initial value, after passing through an intermediate region where the conductivity value remained constant, known as plateau region. The conductivity data were then plotted as a function of the added NaOH volume, as shown in Figure 16. This plot exhibits three distinct sections corresponding to the neutralization of the strong acid (HCl), the weak acid (TOC-COOH), and the excess NaOH.

The equivalence points of the titration are identified by the intersections of the linear segments which represent the regression lines of the 3 regions:

- V_1: This is the intersection between the initial descending segment and the plateau. This volume corresponds to the neutralization of the strong acid (HCl). (Blue line in Figure 15)
- V_2: This is the intersection between the plateau and the final ascending segment. This volume corresponds to the total neutralization of both the strong acid and the weak carboxylic acid groups (TOC-COOH). (Purple line in Figure 15)

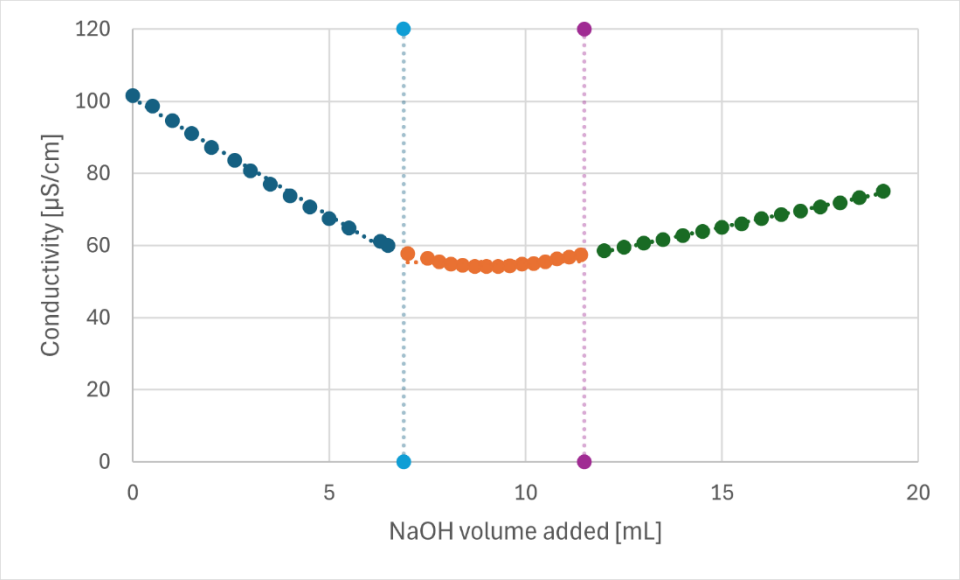

Figure 16: Conductivity titration curve of TOC

Using the Equation 1, it is possible to calculate the amount of the carboxylic groups, expressed as mmol of carboxylic groups per mass of dry TOC ($mmol_{COOH}/g_{TOC}$).

$$[COOH] = \frac{M_{NaOH}\,(V_2 - V_1)}{m_{TOC}} \quad (1)$$

Equation 1: General equation for the calculation of the degree of oxidation of TOC from conductimetric analysis.

M_{NaOH}, V_1, V_2, m_{TOC} represent respectively sodium hydroxide molarity equal to 0.1 M, sodium hydroxide volume added at the beginning of the plateau section, sodium hydroxide volume added at the end of the plateau section, dry mass of the cellulose sample.

2.1.2.2. TOCNF production

Once TOC was obtained, it was dispersed in a mixture of NaOH and deionized water and subjected to ultrasonication, which represents the effective nanosizing step, yielding TEMPO-oxidized cellulose nanofibers (TOCNF).TOC was dispersed in in NaOH 0.1 M (1 equivalent with respect to the mmol of carboxylic groups) and diluted with deionized water to achieve a 2.5% w/w concentration.

The suspension was then ultrasonicated with an immersion ultrasonicator at 0 °C for 5 min, using an ice-bath. After this, a 2.5% w/w suspension of TOCNF was obtained. Subsequently, the solution was acidified with 37% HCl to induce fibres aggregation, facilitating the following vacuum-filtration on a nylon filter with deionized water, until neutral pH was reached. During filtration, the TOCNF suspension was concentrated to a value exceeding 5% w/w. The suspension was kept at around 10°C to preserve its properties.

2.1.3. Functionalization

The introduction of a porphyrinic sensor into the adsorbent material through the functionalization of the main building blocks allowed the incorporation of optical sensors, able to detect specific contaminants.

2.1.3.1. bPEI functionalization

The first incorporation procedure was conducted through the functionalization of bPEI with porphyrinic sensors.

Specifically, 10 mg of porphyrin ($TPPS_4$ or $TPPCH_2$) was completely dissolved in 5 mL of tert-butanol with the aid of a sonication bath. Once a homogeneous solution was obtained, 100 mg of bPEI, either 25 kDa or 1.8 kDa, were added. The reaction was performed in a microwave at 85 °C for 2 hours.

After completion, the reaction mixture was transferred to a dialysis membrane for purification. The membranes used have a molecular weight cut-off of 12-14 kDa for the bPEI 25kDa and 1kDa for the 1.8 kDa. The dialysis was carried out in 2 L of deionized water, which was replaced every 4 hours over a total period of 72 hours.

After dialysis, the solution was transferred to a Falcon tube and frozen. Once completely solidified, the sample underwent freeze-drying to remove residual water. The sample dry mass was then determined by weighing the empty Falcon tube and then reweighing it with the lyophilized sample. Based on the obtained weight, a

functionalized bPEI solution was prepared by dissolving the freeze-dried product in deionized water to achieve a final concentration of 20 mg/mL.

2.1.3.2. Functionalization of cellulose

The second procedure involves the direct functionalization of TOCNF with porphyrin molecules, to incorporate sensing units into the cellulose matrix.

EDC/NHS-mediated amidation

The first approach is an amidation reaction between TOCNF and 1,8-diaminooctane. A carbodiimide-mediated reaction is the most frequent method to amidate cellulose surfaces. The reaction typically targets the carboxylic groups of oxidized nanocellulose substrates. [37]

The first step of the procedure (Figure 18Figure 17) involved the activation of carboxylic groups using 1-Ethyl-3-(3-dimethylaminopropyl)carbodiimide (EDC) and *N*-hydroxysuccinimide (NHS) [60].

Considering 1 g of dry TOCNF with an oxidation degree of 1.5 $mmol_{COOH}/g_{TOCNF}$ as reference, 25 molar equivalent of EDC and 8.7 molar equivalent of NHS respect to the carboxylic moieties were added into a beaker containing 50 mL of a TOCNF aqueous suspension. The solution was put into ice bath and stirred for 30 minutes, allowing the carboxyl groups on the cellulose to be activated for the subsequent amidation reaction.

In a separate beaker, 380mg of sodium carbonate (Na_2CO_3) and 2 equivalents of 1,8-diamminooctane with respect to the carboxylic moieties of the cellulose were dissolved in 50 mL of deionized water and maintained under stirring. The solution containing the diamine was then slowly combined with the activated TOCNF suspension, and the reaction mixture was stirred at room temperature for 48 hours, enabling the formation of covalent amide bonds between the cellulose carboxyl groups and the 1,8-diaminooctane.

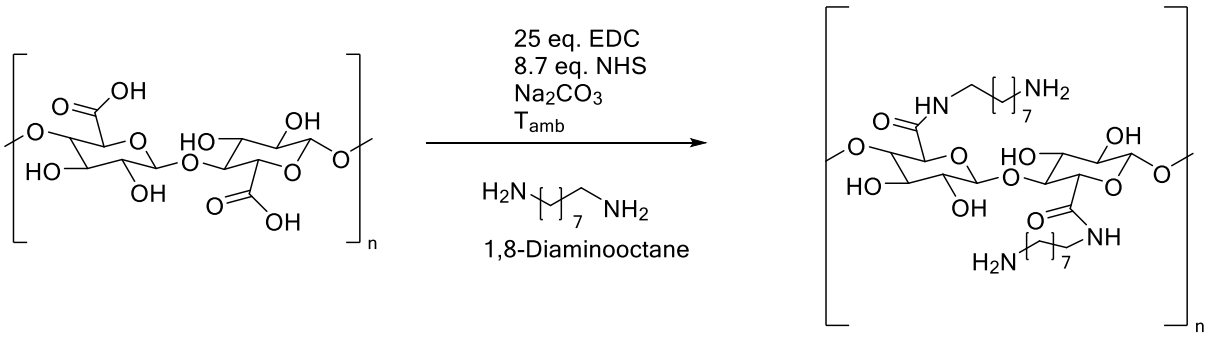

Figure 17: Route synthesis of amino-functionalized TOCNF

After 48 hours,, the reaction was terminated, and the product was subjected to a work-up to remove any unreacted reagents and by-products. The work-up began with a Büchner filtration to separate the solid amino-functionalized TOCNF from the reaction

medium. The collected material was then sequentially washed to ensure complete purification with: 0.1 M sodium hydroxide, 0.1 M hydrochloric acid, deionized water, methanol and acetone. Each washing step was repeated three times to ensure complete removal of residual reagents. Finally, the amino-functionalized TOCNF were washed suspended in deionized water and stored in the form of an aqueous suspension at 10°C under refrigeration.

To analyse the outcome of the amidation reaction, an elemental analysis was performed and further discussed in 3.2.2.

The functionalization of the amino-modified TOCNF with $TPPCH_2$ was carried out following the same amidation procedure previously described. In this process, 250 mg of amino-functionalized TOCNF were dispersed in a mixture containing 220 mg of $Na_2CO_3$and 14.5 mL of deionized water. In a separate beaker, 10 mg of $TPPCH_2$ were dispersed together with 60.86 mg of EDC and 12.7 mg of NHS in 10 mL of deionized water, and the mixture was kept under magnetic stirring in an ice bath for 30 minutes. After activation, the $TPPCH_2$ solution was added to the TOCNF suspension, and the reaction was allowed to proceed under continuous stirring to promote coupling between the porphyrin and the nanofibrils.

After 48 hours, the work-up procedure was carried out as described in Section EDC/NHS-mediated amidation. Again, the purified product was suspended in deionized water and stored in the form of an aqueous suspension at 10°C under refrigeration.

APTES

The second approach is the silytation reaction between (3-Aminopropyl)triethoxysilane (APTES) and TOCNF. Silylation, also known as silane grafting, has proven to be an effective way to change cellulose surfaces. Silanes used to treat cellulose possess distinct functional groups at each end, allowing one end to interact with the hydroxyl groups of cellulose and the other end to react with functional groups in the matrix, thereby forming a bridge. APTES is one among the most used silanes due to its simple structure and low cost. [61]

Different procedures for the incorporation of (3-Aminopropyl)triethoxysilane (APTES) into cellulose are being examined.

The first procedure (Figure 18) involves TOCNF functionalization following a procedure reported in the literature, with minor modifications [62]. Briefly, 1 g of TOCNF was dispersed in a beaker containing 100 mL of 90% aqueous ethanol solution (final concentration of 1 wt%). Meanwhile, 240 mg of APTES were dispersed in 10 mL of 80% aqueous ethanol solution, and the mixture was added to a three-necked flask equipped with a mechanical stirrer, thermometer, and condenser, and heated at 50 °C under continuous stirring for 1 h. The pH of the TOCNF suspension was adjusted to 4

using glacial acetic acid. The acidic suspension was then poured into the flask and stirred for 2 h. The resulting product was washed three times by centrifugation in ethanol at 4000 rpm for 15 minutes each cycle. Finally, the sample was left to dry overnight at room temperature. The obtained product is designated as TOCNF-APTES1.

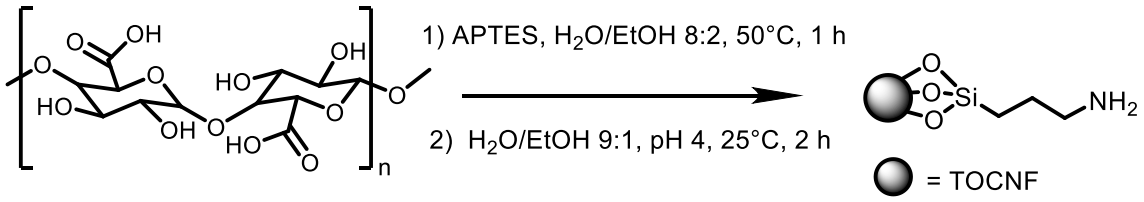

Figure 18: First route synthesis of APTES-functionalized TOCNF

The second procedure, illustrated in Figure 19, involves the reaction of TOCNF with APTES in equal quantities [63]. A 10% (v/v) APTES solution was prepared in ethanol, while TOCNF were dispersed in deionized water at a 1 % w/w . Both solutions were stirred separately for 10 minutes. The APTES solution was then added dropwise to the TOCNF dispersion under continuous stirring. The pH of the mixture was adjusted to 10 using 1 M NaOH. The reaction was maintained under stirring at room temperature for 2 hours, followed by heating at 80 °C for additional 3 hours. The resulting product was purified by three sequential centrifugation cycles at 6000 rpm for 5 minutes each, using a 50 % v/v aqueous ethanol solution. The obtained product is nominated as TOCNF-APTES2.

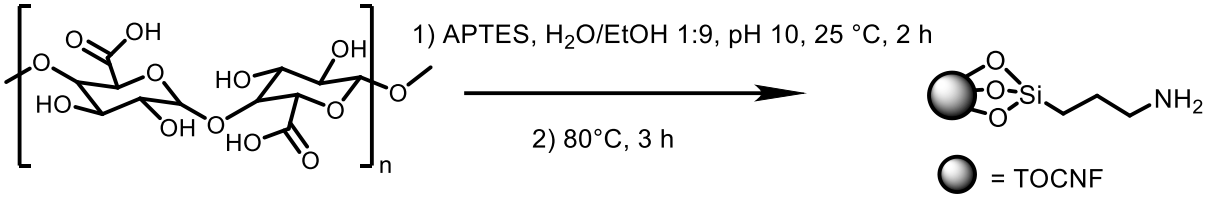

Figure 19: Second route synthesis of APTES-functionalized TOCNF

The third procedure, illustrated in Figure 20, involves TOCNF functionalization as reported in the literature, with minor modifications [64]. Initially, 1 g of TOCNF was dispersed in 100 mL of deionized water containing 1.5 g of NaOH and 6 g of urea. The suspension was vigorously stirred at 0°C for 6 hours. Subsequently, 5 mL of APTES were dissolved in 25 mL of deionized water and added to the TOCNF suspension. The reaction mixture was stirred at room temperature for 24 hours. The resulting product was then filtered, washed successively with deionized water and ethanol, and dried to obtain the functionalized sample TOCNF-APTES3.

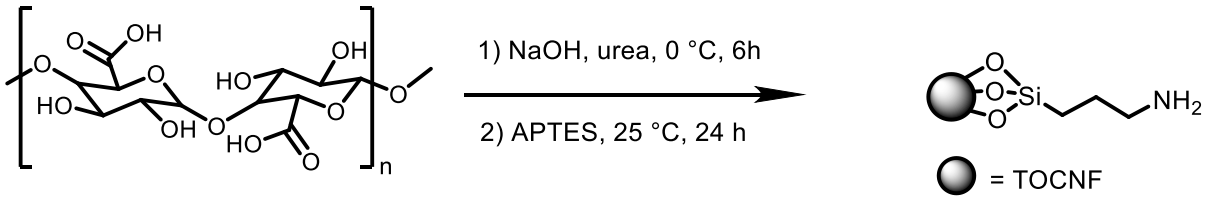

Figure 20: Third route synthesis of APTES-functionalized TOCNF

2.1.4. Production of Cellulose Nanosponges

Once the TOCNF have been obtained, the next step involved the preparation of cellulose nanosponges (CNS), presented in Figure 21. Several formulations of CNS were developed and compared. Although the specific compositions may vary, the overall production process can be summarized in four main stages:

1. mixing of the components to ensure homogeneous dispersion,
2. freeze-drying to obtain a porous, sponge-like structure,
3. thermal treatment to promote crosslinking and structural stability,
4. washing to remove any unreacted reagents or impurities.

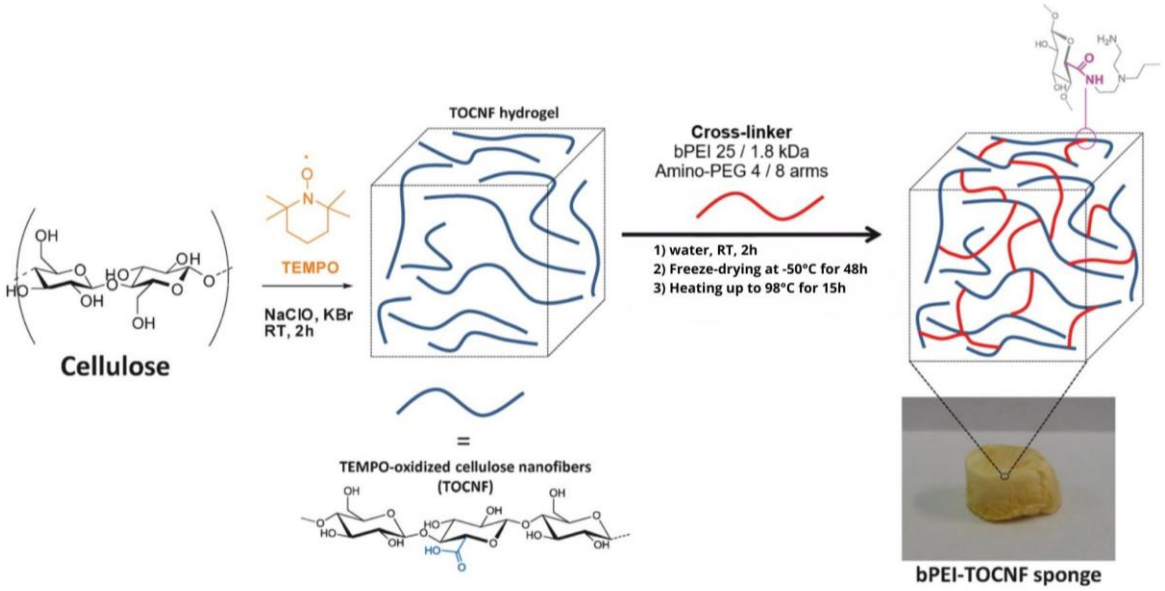

Figure 21: CNS synthesis process

Considering 1 g of dry TOCNF as the reference, the compositions of all CNS batches are summarized in Table 1. The formulations are expressed as TOCNF-to-branched polyethylenimine (bPEI) mass ratios. Deionized water was added to each batch to achieve a final dry content of 3% w/v in the CNS formulation.

	TOCNF	bPEI 25 kDa	bPEI 1.8 kDa	Citric Acid
1:2	1g	2g	-	-
1:0.5	1g	-	0.5g	-
1:1:18	1g	1g	-	0.256g

Table 1: CNS formulations

For the production of the different CNS formulations, two molecular weight variants of bPEI, 25 kDa and 1.8 kDa, have been employed.

In the TOCNF–water mixture, cross-linkers were added dropwise under continuous agitation to promote uniform dispersion of the polymer within the suspension. Once a homogeneous mixture was achieved, it was carefully transferred into a pre-refrigerated metallic mold using a plastic pipette. The mold was maintained at −20 °C to allow complete freezing of the CNS nanostructure.

Following solidification, the frozen sample was subjected to lyophilization at −50 °C and 140 μbar for 48 hours to remove residual water and obtain a dry, porous CNS structure. Then, the lyophilized samples were thermally treated in a controlled process, where the temperature was gradually increased from 68 °C to 98 °C in 10 °C increments. Each temperature step was maintained for 45 minutes, except for the final step at 98 °C, which was held for 15 hours to ensure structural stabilization of the material.

Finally, the CNS samples were thoroughly washed five times with deionized water and once with ethanol to eliminate any unreacted reagents or residual impurities.

2.1.5. Cellulose nanosponges functionalization with porphyrins

Porphyrin sensor can be introduced into CNS formulations to introduce a detection property. The porphyrinic molecules are introduced in two different ways: direct mixing or functionalization.

Focusing on direct mixing method, a defined amount of porphyrin were dissolved in deionized water with the help of a sonicator bath until complete solubilization. This solution was then incorporated during the mixing step together with bPEI-TOCNF mixture.

On the other hand, the functionalization method consists of functionaling one of the CNS building blocks with the porphyrin molecule. The functionalization can happen on the bPEI or on TOCNF, as mentioned in 2.1.3. The amount of bPEI introduced as the functionalized component was subtracted from the total cross-linker amount, calculated as the mass equivalent relative to the TOCNF mass. Similarly, the amount of functionalized TOCNF used was adjusted according to the required sensor content.

The synthesis procedure for the functionalized CNS followed the same approach described in paragraph 2.1.4.

Different porphyrin-to-TOCNF ratios were investigated in order to evaluate the influence of the sensor loading on the materials. The corresponding formulations are summarized in Table 2. Each CNS formulation was prepared according to the TOCNF–bPEI ratios describedTable 1, and porphyrin is subsequently incorporated at three different porphyrin-to-TOCNF mass ratios (1:200, 1:100, and 1:50), corresponding to 5, 10, and 20 mg of porphyrin per gram of TOCNF, respectively.

CNS Code	Crosslinker	Ratio TOCNF:bPEI	Sensor Incorporation Method	Porphyrin Molecule	Sensor (ratio)
LDV15	bPEI 25 kDa	1:2	Functionalized bPEI	$TPPCH_2$	1:200/1:100/ 1:50
LDV16	bPEI 25 kDa	1:2	Functionalized bPEI	$TPPS_4$	1:200
LDV26	bPEI 1.8 kDa	1:0.5	Direct mixing	$TPPS_4$	1:200/1:100
LDV27	bPEI 25 kDa	1:2	Direct mixing	$TPPS_4$	1:200/1:100
LDV28	bPEI 1.8 kDa	1:0.5	Direct mixing	$TPPCH_2$	1:200/1:100
LDV29	bPEI 25 kDa	1:2	Direct mixing	$TPPCH_2$	1:200/1:100
LDV40	bPEI 1.8 kDa	1:0.5	Functionalized bPEI	$TPPCH_2$	1:200/1:100
LDV41	bPEI 1.8 kDa	1:0.5	Functionalized bPEI	$TPPS_4$	1:200

LDV44	bPEI 25 kDa	1:2	Direct mixing	SiTTC	1:200/1:100
LDV45	bPEI 1.8 kDa	1:0.5	Direct mixing	SiTTC	1:200/1:100
LDV8	PEG 8 arms*	1:0.5	Direct mixing	SiTTC	1:200/1:100
LDV9	bPEI 25 kDa	1:2	TOCNF functionalization (1,8-diaminooctane)	$TPPCH_2$	1:200
LDV10	bPEI 1.8 kDa	1:0.5	TOCNF functionalization (1,8-diaminooctane)	$TPPCH_2$	1:200

Table 2: Functionalized CNS formulations

*CNS containing amino-polyethylene glycol (amino-PEG) 8 arms were prepared following the same synthesis route of the bPEI-based CNS.

2.2. Analysis of materials

2.2.1. CNS analysis with SEM

To characterize the newly developed CNS formulations, specifically LDV8, LDV9, LDV10, LDV44, and LDV45, a scanning electron microscope (SEM) analysis has been performed.

SEM analysis produces highly magnified images, highlighting size, shape, composition, crystallography and other chemical and physical properties of the sample. The material is analysed with an electron beam generated in a vacuum environment. Images are formed by detecting electrons emitted or reflected from the sample surface during beam interaction. [65]

SEM analysis of CNS was performed using a variable pressure instrument (SEM Cambridge Stereoscan 360) at 100/120 pA equipped with a BSD detector. The operating

voltage was 15 kV with an electron beam current intensity of 100 pA. The focal distance was 9 mm.

2.2.2. Characterization of functionalized cellulose

To characterize functionalized TOCNF, an elemental analysis was performed for TOCNF-1,8diaminooctane and an Inductively Coupled Plasma (ICP) Spectroscopy and Attenuated total reflection Fourier transform infrared spectroscopy (ATR-FTIR) for TOCNF-APTES.

Elemental analysis is an analytical technique applied in chemistry to determine the elemental composition of chemical compounds and their composites. Through this method, it can be determined which elements, in particular carbon, hydrogen, nitrogen and sulphur, are present and mass percentage of each chemical element contained in the tested products. [66]

ICP Spectroscopy (ICP/OES analysis (Perkin Elmer Optima 8300) is an analytical method for detecting and measuring elemental composition in chemical samples, particularly metals and metalloids. The method is based on the ionization of a sample by an extremely hot plasma, usually made from argon gas. [67]

Infrared spectroscopy analyses the interaction of infrared light with matter. When infrared light passed through a sample, the wavelengths absorbed are dependent on the molecular vibrations of the substance. Consequently, based on the wavelength absorbed, it is possible to obtain both chemical and structure of the sample [68]. The analysis was performed using an iS50 ATR-FTIR spectrophotometer from Thermo Fischer Scientific.

The aim of these analyses was to evaluate the efficiency of the functionalization reactions, quantify the amount of amine groups introduced into cellulose and compare the different APTES functionalization methods to identify the most effective procedure.

2.3. Preliminary tests for colorimetric detection of PFOA

Preliminary tests were performed to evaluate the colorimetric response of PFOA in aqueous solution of the SiTTC-functionalized CNS. Different concentrations were tested: 50, 100, 200, 500 and 1000 ppm.

The starting solution (1 g/L) containing PFOA was prepared by dissolving 1 g of PFOA solid salt respectively in 1 L of PBS solution. The PBS solution was prepared dissolving 9.6 g of Dulbecco's Phosphate Buffered Saline in 1 L of deionized water. All subsequent solution were prepared by appropriate dilution with PBS solution.

CNS samples were inserted in clean plastic Falcon® vial with 20 mL of the solution at the desired concentration. The samples were kept under orbital shaking at 200 rpm for 24 hours. CNS were removed from the solution, and the test results were assessed by visual inspection of the wet nanosponge.

3 Results and Discussion

3.1. CNS production process

The aim of this work was to produce a cellulose-based porous material combining both adsorption and detection properties. To achieve this goal, various formulations were tested to evaluate the most effective ones in terms of detection performance while maintaining strong contaminant adsorption capacity.

First of all, two different procedures for the TEMPO-mediated oxidation reaction were evaluated. It was observed that once the pH is stable, the reaction can be considered complete. Prolonging the reaction overnight results in the minimal conversion of few hydroxy groups. Therefore, the reaction time can be stopped when the pH stabilizes. Nevertheless, the rheological properties of the TEMPO-oxidized cellulose varies according to the method used.

The carboxylic content of both TEMPO-oxidized cellulose samples was determined through conductimetric titration, producing results between 1-1.5 $\frac{mmol_{COOH}}{g_{TOC}}$. The carboxylic moieties are necessary for the crosslinking reaction with the amino groups of the crosslinking agents, guaranteeing the mechanical stability, integrity and porosity of the composite material.

To ensure proper fibres dispersion during ultrasonication, 0.1 M NaOH was added to promote a homogenous distribution. The required volume of NaOH was calculated based on the carboxylic units present in the suspension, maintaining an equimolar ratio between sodium hydroxide and carboxylic unit.

Two different cross-linkers, branched polyethyleneimine (bPEI) and eight-arms polyethylene glycol (PEG 8-arms), were tested to evaluate the different properties in the CNS. For the production of the different CNS formulations, two molecular weight variants of bPEI, 25 kDa and 1.8 kDa, have been employed, in order to examine the influence of polymer molecular weight on the resulting material properties.

Both cross-linkers contain a sufficient amount of amino groups, capable of forming amide bonds with the carboxylic groups of the cellulose nanofibers. Moreover, the terminal amine groups can further react with porphyrin-based sensors, enabling their functionalization within the CNS structure.

In the 1:1:18 formulation, citric acid functions as co-crosslinker and its amount corresponds to 18% of the total molar amount of amino groups in bPEI. The addition of citric acid prevents the release of bPEI during water treatment and increases CNS chemical and mechanical stability. [36]

The two porphyrinic sensors detecting mercury, supplied by the University of Roma – 'Tor Vergata', have the same core structure but different peripheral functional groups. $TPPCH_2$ is easily incorporated into CNS through chemical bonding, as the carboxylic moieties of the sensor react with the primary amino groups of the cross-linker. Similarly, $TPPS_4$ is integrated into the CNS by reacting the sulfonic group with the amino group. However, $TPPS_4$ showed a hydrophobic behaviour, suggesting that not all sulfonic groups reacted with the amino groups and that part of the sensor was instead physically entrapped within the cellulose matrix.

Each step of the preparation process is crucial to obtain a homogeneous final product. The mixing step is fundamental to ensure uniform dispersion of TOCNF, cross-linker, and sensor. In particular, the incorporation of the sensor is essential, as inhomogeneous distribution can lead to variations in the colorimetric response throughout the CNS.

The resulting suspension is then transferred into a cylindrical metallic mould using a plastic pipette. The samples undergo a freezing step. The freezing temperature plays an important role in determining the final morphology of the material, as slower freezing promotes the formation of larger ice crystals, which during the freeze-drying process generate larger and more accessible pores. This step is particularly important for obtaining a porous structure that facilitates contaminant diffusion and adsorption.

Freeze-drying is employed to eliminate water from the sponges while maintaining their three-dimensional structure. Subsequently, the sponges are subjected to thermal treatment to promote the formation of amide bonds between the cellulose and the cross-linker. The temperature is maintained below 98 °C to prevent thermal degradation of the heat-sensitive materials.

To remove any unreacted reagents, the obtained CNS are washed and subsequently air-dried. However, CNS functionalized with the porphyrinic molecules are not washed because the 3D structure is not preserved upon drying.

Different incorporation methods were tested to introduce the porphyrinic sensors inside the CNS: direct mixing, functionalized cross-linker (bPEI) and functionalized cellulose. Analysing any losses of the sensor in the process is crucial to improve the reaction efficiency.

In the direct mixing process (section 2.1.4), no significant sensor losses were observed because the sensor is directly incorporated in the cellulose-cross-linker suspension.

Instead, in both functionalization strategies, partial sensor losses were noticed. In the functionalization of bPEI, described in section 2.1.3.1, the microwave reaction did not achieve completeness. This was evident during dialysis, as the washing water exhibited coloration corresponding to unreacted sensor, sometimes persisting even after 72 hours.

Similarly, in the cellulose functionalization, described in section 2.1.3.2, the amidation reaction did not achieve complete yield. During the work-up of 1,8-diaminooctane-modified cellulose reacted with $TPPCH_2$, significant amounts of sensor were removed during washing, as indicated by the persistent red coloration of the washing solution

These observations confirm that functionalization occurs, but also highlight the need for further optimization, particularly in determining the appropriate sensor loading and improving reaction yields.

3.2. Mercury

3.2.1. Flow-through tests

Building on the preliminary colorimetric and adsorption results reported in the thesis of Davide Luzzini [70], flow-through experiments were designed to more accurately evaluate the performance of CNS. These tests specifically aim to assess the detection capability of CNS under continuous-flow conditions, thereby better mimicking realistic scenarios in which contaminated water passes through a functionalized detecting material.

This approach enables the investigation of material behaviour under dynamic conditions, where adsorption and sensing occur simultaneously during water permeation. In particular, the experiments focus on monitoring the progressive colorimetric response of the CNS as mercury accumulates within the porous network.

The ultimate objective is to determine the detection-based saturation of the material, defined as the point at which a stable and irreversible colour change is observed. This endpoint corresponds to the presence of a specific amount of mercury retained within the sponge, which can be directly correlated with the quantity adsorbed. Through this strategy, flow-through testing provides a more realistic assessment of both sensing performance and adsorption capacity, supporting the development of CNS materials suitable for smart water remediation applications.

3.2.2. Functionalization of cellulose for sensing applications

In previous studies [70], CNS, composed of cellulose and bPEI as the two main building blocks, were prepared using bPEI functionalized with a porphyrin-based sensor, so that the sensing functionality was confined to the cross-linking component rather than the cellulose framework. CNS prepared with functionalized bPEI showed significant detection properties. However, the colorimetric variation was observed from 200 ppm, a relatively high level of ppm considering the typical quantity of mercury present in water.

For this reason, we explored an alternative strategy aimed at enhancing the material's sensitivity by functionalizing the other main building block of the CNS, cellulose.

Different cellulose functionalization strategies, described in detailed in section 2.1.3.2, were explored to assess the performance and stability of incorporating the porphyrin molecule directly onto the cellulose backbone, in comparison with its introduction into CNS through reaction with the functionalized bPEI.

3.2.2.1. EDC/NHS

This paragraph presents the results of the amidation reaction, which is described in the Section entitled EDC/NHS-mediated amidation.

To characterize the final product, elemental analysis was performed to assess the efficiency of the amidation reaction. The degree of substitution (DS), which represents the number of amine groups introduced per anhydroglucose unit (AGU), was calculated according to a procedure described in the literature [70].

First of all, TOCNF have been characterized through the elemental analysis, calculating the degree of oxidation as reported in **Errore. L'origine riferimento non è stata trovata.**:

$$DO_{elemental\ analysis} = \frac{M(C)_{AGU} - \%C\ x\ M_{AGU}}{\%C\ x\ (M_{AGU-COONa} - M_{AGU})} \quad 2$$

Equation 2: General equation for the calculation of the degree of oxidation of TOCNF from elemental analysis results.

Where $M(C)_{AGU}, \%C, M_{AGU}$ and $M_{AGU-COONa}$ correspond to the molecular mass of carbon in an AGU (72.04 g/mol), the carbon content in TOCNF sample obtained by elemental analysis, the total molar mass of an AGU (162.14 g/mol), and the molar mass of an oxidized AGU with sodium salt as counter ion (35.93 g/mol), respectively.

Moreover, the degree of substitution can be calculated according to Equation 3:

$$DS_{elemental\ analysis} = \frac{\%N\ x\ (M_{AGU} + DO\ x\ (M_{AGU-COONa} - M_{AGU})}{M(N)_{grafted} - \%N\ x\ M_{grafted}} \quad 3$$

Equation 3: General equation for the calculation of the degree of substitution of modified TOCNF after amidation calculated from elemental analysis results.

Where the terms M_{AGU} and $M_{AGU-COONa}$ are equal to those used in **Errore. L'origine riferimento non è stata trovata.**; terms %N, $M(N)_{grafted}$, and $M_{grafted}$ correspond respectively to the nitrogen content in modified TOCNF sample obtained by elemental analysis, the nitrogen molar mass of grafted moieties (28.0 g/mol), and the total molar mass of the grafted moieties (144.26 g/mol). DO is the degree of oxidation, corresponding to the number of carboxylic groups per AGU. OD of TOCNF could be calculated from the titration curves according to Equation 4:

$$DO = \frac{M_{AGU}\ x\ C\ x\ (V_2 - V_1)}{w - 36\ x\ C\ x\ (V_2 - V_1)} \quad 4$$

Equation 4: General equation for the calculation of the degree of oxidation (DO) of TOCNF

In Equation 4, C corresponds to the exact NaOH concentration (mol/L), V_1 is sodium hydroxide volume added before the plateau section, V_2 is sodium hydroxide volume added after the plateau section, w is the dry amount of TOCNF (g), M_{AGU} is equal to those used in **Errore. L'origine riferimento non è stata trovata.**, and 36 g/mol corresponds to the difference between the molar masses of an AGU and the sodium salt of a glucuronic acid moiety.

	%C	%N	$DO_{elemental\ analysis}$	DO	$DS_{elemental\ analysis}$
TOCNF	43.56	< 0.01	1.27	1.63	-
TOCNF-1,8-diaminooctane	49.58	9.54	1.27	1.63	0.31

Table 3: Result from elemental analysis

These results, shown in Table 3, imply that 55% of the carboxylic groups on the TOCNF have been successfully linked to the ammine groups of the 1,8-diaminooctane, resulting in a DS of 0.53 $mmol_{NH_2}/g_{TOCNF}$, according to the conductimetric titration. Only 10% of the pendant primary amino groups will be functionalized with the porphyrinic sensor.

The only porphyrin used in this method is the $TPPCH_2$ because is the only one bearing carboxylic groups. These carboxylic groups can react with primary amines, leading to the formation of amide bonds. On the other hand, $TPPS_4$ contains sulfonic groups; therefore it cannot undergo the same coupling reaction. Using the procedure described in **Errore. L'origine riferimento non è stata trovata.** section, the carboxylic groups of $TPPCH_2$ can react with the amino ones of the 1,8diaminooctane-functionalized cellulose. For a molecule of $TPPCH_2$, only one carboxylic acid can react with the primary amine.

SEM analysis

The 1,8-diaminooctane-functionalized CNS modified with $TPPCH_2$ were analysed through SEM analysis to evaluate the morphology and the porosity. For each sample, the inner and external sides were examined. Only one CNS for each batch was analysed, assuming minimal differences between all the samples. Additionally, to observe the internal structure, the samples were sectioned by applying mechanical pressure, which may have altered the initial morphology of the sponges.

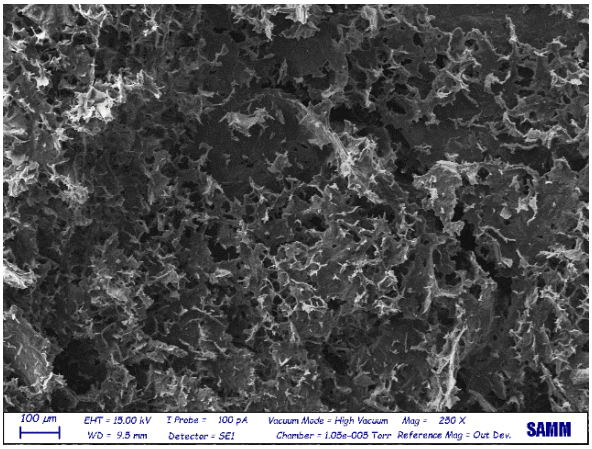

Internal side LDV 9

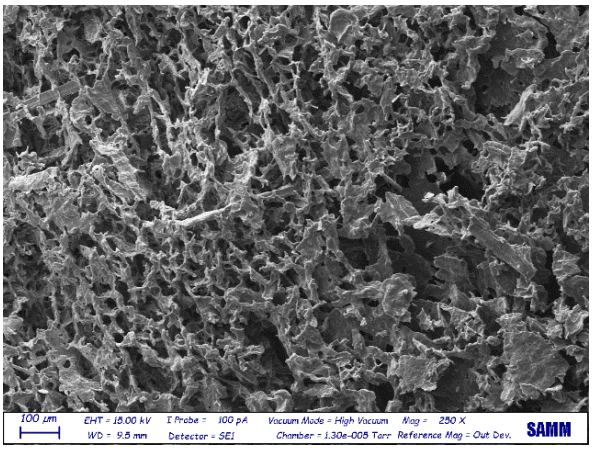

External side LDV 9

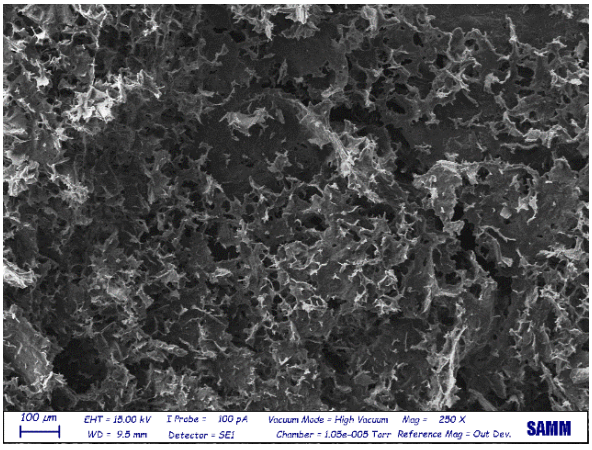

Internal side LDV 10

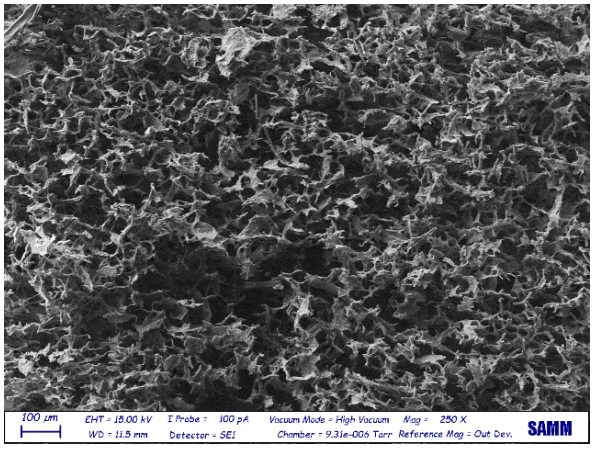

External side LDV 10

Figure 22: SEM analysis of cellulose-functionalized CNS

All the images illustrated in Figure 22 show a highly porous, three-dimensional network structure with irregular cavities and channels of varying sizes. The size of pores ranges throughout the sample.

Overall, the image confirms the presence of a porous structure that could facilitate diffusion and surface interactions within the material.

The porosity of the sponges is calculated as area fraction, using the software ImageJ. The results are shown in Table 4.

CNS type	Magnitude	Scale [μm]	Internal porosity	External porosity
LDV 9	250X	100	21.15% (2)	35.89% (2)
	500X	20	24.85% (3)	30.89% (3)
	250X	100	23.70% (5)	34.74% (5)
	500X	20	22.32% (6)	36.80% (6)
LDV 10	250X	100	26.52% (2)	27.64% (2)
	500X	20	28.45% (3)	25.83% (3)
	250X	100	31.59% (5)	30.35% (5)
	500X	20	20.32% (6)	20.31% (6)

Table 4: Functionalized-cellulose CNS porosity data

The internal porosity is lower than the external porosity, which can be explained analysing the freeze-drying process. Crystal formation starts from the outer layer of the cellulose-based sponge. Consequently, the outer region, exposed to lower temperature, develops larger macropores while inner layers are structurally confined, less able to expand, leading to tighter fiber packing and reduced void space.

The high porosity of the external layer allows faster contaminant penetration by having more accessible pathways. Consequently, the diffusion rate is higher in the external region of the CNS. On the other hand, the small pores in the inner region reduce the diffusion coefficient. However, the more structured internal region provides structural stability to the material.

CNS type	**Magnitude**	**Scale** [μm]	**Porosity**
bPEI 1.8 kDa CNS TPPCH2	500	20	13.43

bPEI 25 kDa CNS TPPCH2	500	30	27.47

Table 5: Porosity data of CNS

The porosity values reported in Table 5 are based on previous studies conducted by the O^{SCM} Lab. In those works, CNS were synthesized using functionalized branched polyethyleneimine (bPEI) as a cross-linking agent.

Comparing the CNS prepared in this work using functionalized cellulose, the previously reported CNS display lower porosity. A possible explanation for this porosity difference is the introduction of 1,8-diaminooctane in the new formulations. 1,8-diaminoctane has a relatively long aliphatic chain that can impose spatial constraints during the network formation. Additionally, it can introduce steric hindrance effects. These steric effects may increase intermolecular distances with the polymeric matrix, leading to a more open porous structure.

Therefore, the functionalization of cellulose leads to an increased porosity due to the incorporation of long aliphatic chains. The higher porosity may enhance contaminant accessibility to sensing sites, improving the colorimetric response at lower pollutant concentrations.

3.2.2.2. APTES

This paragraph presents the results of the various silylation reactions, all of which are described in detail in Section APTES.

ICP-OES analysis

To evaluate the most effective APTES integration reaction in the cellulose matrix described in the Section **Errore. L'origine riferimento non è stata trovata.**, an ICP-OES analysis is performed in which the quantity of the silicon is calculated.

	TOCNF-APTES1	TOCNF-APTES3
Silicon quantity (%w per g of cell)	1.92%	3.24%
DS	0.11	0.18

Table 6: ICP-OES analysis results

The degree of substitution (DS) has been simply calculated using the following formula:

$$DS = \frac{n_{APTES}}{n_{AGU}} = \frac{m_{Si}}{MM_{Si}} \frac{m_{cell}}{MM_{AGU}} \quad 5$$

Equation 5: General equation for the calculation of the degree of substitution

Where m_{Si}, MM_{Si}, m_{cell}, MM_{AGU} represent respectively the quantity of silicon present in the sample ($\frac{g_{Si}}{g_{cell}}$), the molecular of silicon equal to 28.085 g/mol, the mass of the cellulose sample, the total molar mass of an AGU (162.14g/mol).

As shown in Table 6, the silylation process has happened in all three cases. The third procedure introduced more silane into the TOCNF matrix. The higher quantity of APTES leads to a greater quantity of terminal amino groups, promoting the subsequent cross-linking reactions.

Additionally, besides the bonding between the silane and the TOCNF hydroxy groups, APTES is prone to self-polymerization. This process leads to the formation of a robust siloxane (Si-O-Si) network, increasing effectively the availability of amino groups and the material adsorption capacity [71].

A further improvement is to develop functionalized CNS sponges by introducing amino groups through APTES. These amino groups can react with the carboxylic ones of the $TPPCH_2$ porphyrinic sensor. Subsequently, CNS can be synthesized using APTES-functionalized TOCNF and the cross-linker, following the procedure described in 2.1.4.

ATR-FTIR analysis

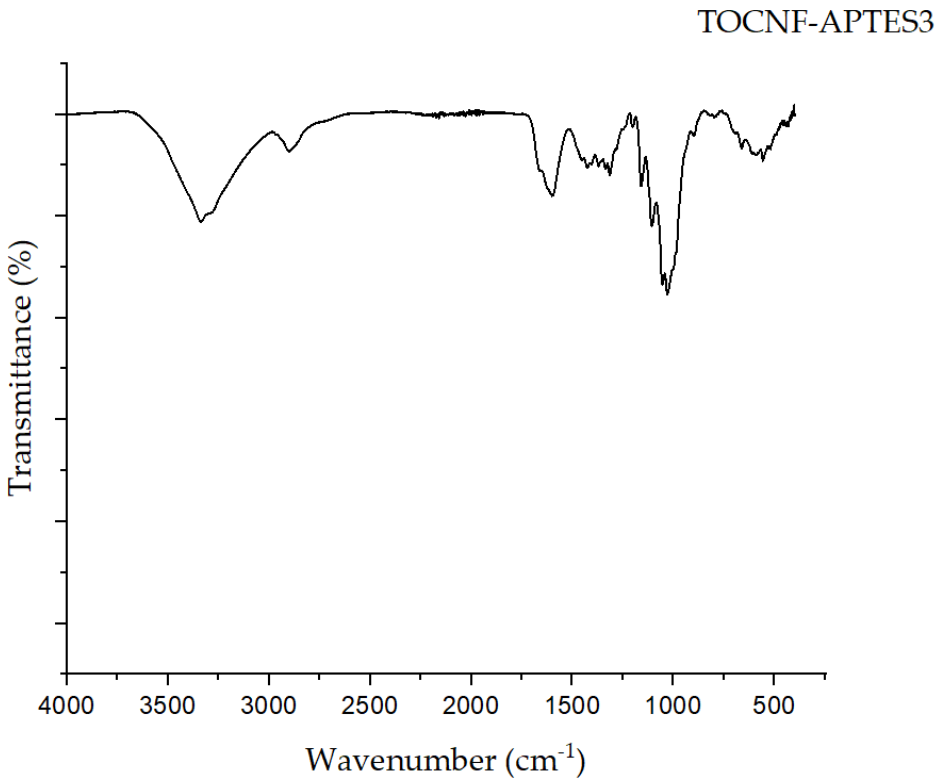

Figure 23: ATR-FTIR analysis of TOCNF-APTES3 sample

The FTIR spectrum, shown in Figure 23, confirm the functionalization of TOCNF with APTES. The peak at around 1100-1000 cm^{-1} is attributed to Si-O-Si and Si-O-C bonds stretching vibration, indicating the formation of bond between the silane group and TOCNF. Furthermore, the characteristics bands of TOCNF are preserved. The peak at around 1700 cm^{-1} shows the stretching vibration of C=O, showing the effectiveness of TEMPO-mediated oxidation. In the 3500-3000 cm^{-1} range, the stretching of O-H bonds due to cellulose and, possibly, N-H vibrations introduced by APTES are shown.

3.2.3. Comparison with literature

In literature, there is another example of cryogel able to detect and remove mercury, produced by Salanitri et al. [72]. In this study, a methacrylic acid (MAA) based macroporous material functionalized with thiol groups is synthetized for the removal and detection of mercury ions from water.

The synthesis of this material can be summarized into three main steps. The first step is the synthesis of porphyrin acrylate monomer (PORPH-acrylate). Meso-tris(N-methyl-4-pyridyl) mono (4-carboxylphenyl) porphine trichloride (PORPH) reacts with 2-Aminoethyl methacrylate hydrochloride (AEMA) using N,N'-Dicycloexylcarbodiimide (DCC), 1-Hydroxy benzotriazole (HOBT), N-Methyl morpholine (NMMO) in anhydrous N,N-Dimethylformamide (DMF) as coupling agents. The product is then purified by centrifugation.

The second step is the synthesis of methacrylic acid based-PORPH cryogel (MAA-PORPH) through cryopolymerization at -15°CMAA reacts with N,N'-methylene-bis-acrylamide (MBAA) and PORPH-acrylate, in water. The catalytic system used to initiate the cryopolymerization is formed by a TEMED and APS solution.

Finally, the material is functionalized with thiol groups. The MAA-PORPH carboxyl groups are activated by reacting with DCC, HOBT and NMMO in anhydrous DMF. Then the activated MAA-PORPH reacted with cyst-amine hydrochloride (CYS), NMMO, HOBT in anhydrous DMF. This step forms amides containing disulfide bridges. The disulfide bridges are cleaved using 3-mercapto-1,2-propanediol (MPD) to generate the final THIOL-PORPH cryogel.

SEM analysis confirmed an interconnected macroporous network with pore sizes between 3–23 μm, showing that the functionalization does not compromise the macroporous structure.

The adsorption performance of THIOL-PORPH was evaluated through a series of adsorption tests for Hg(II). The material was immersed in aqueous solutions at different mercury concentrations, ranging from 100 to 1500 ppm, for 36 hours. The maximum adsorption capacity was reached between 500 and 1500 min. The material achieved an exceptional mercury maximum adsorption capacity exceeding 1000 mg/g. As shown in Figure 24, the experimental data are fitted by Langmuir isotherm (red curve) and Freundlich isotherm (blue curve), confirming the high adsorption.

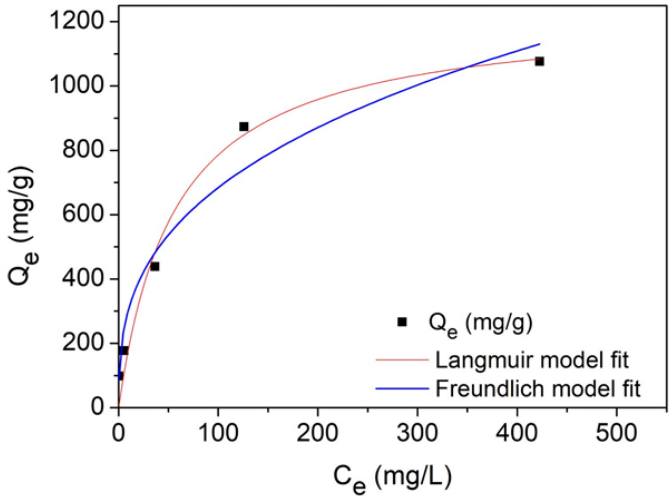

Figure 24: Equilibrium adsorption Langmuir (red curve) and Freundlich (blue curve) isotherm for THIOL-PORPH cryogel [72]

Furthermore, selectivity toward mercury was tested. In the presence of equimolar quantities of multiple metal ions, particularly Pb(II), Zn(II), Co(II), Cu (II), and Ni(II), the material demonstrated a 95% mercury selectivity.

Although the material exhibits excellent performance in mercury removal and offers the innovative advantage of visual saturation monitoring, from a sustainability point of view, several critical issues emerge.

First of all, the cryogel is formed by acrylic polymers, produced mainly from fossil sources and therefore generally not biodegradable [73]. This may contribute to contaminant release, making the material unsuitable for sustainable environmental remediation.

Regarding the synthesis step, several reagents are toxic and require environmentally intensive production. For example, DMF is a highly toxic organic solvent, making the synthesis of the THIOL-PORPH cryogel particularly challenging from both environmental and safety perspectives. Moreover, the extensive use of organic solvents, relative to reagents, requires multiple extraction, purification, and cleaning steps to achieve adequate product purity. This excessive consumption of non-renewable and hazardous solvents represents a significant environmental concern and highlights the unsustainability of the process.

Furthermore, the synthesis requires high energy input, particularly for maintaining the low temperatures needed for cryopolymerization and for drying processes under nitrogen flow and vacuum conditions. These steps significantly increase the overall energy demand and carbon footprint of the material.

In contrast, cellulose-based materials are derived from renewable and environmentally friendly resources. Most of the reagents used in their synthesis are

non-toxic and biodegradable. Additionally, water is typically employed as the reaction medium, minimizing environmental risks and ensuring high availability and sustainability.

Moreover, porphyrin molecules allow mercury detection through colorimetric variation.. However, the thiol groups possess a higher affinity for mercury ions respect to the porphyrin molecules. Due to this quality, thiol groups bind to mercury first. Once the thiol groups are approximately 70% saturated, the mercury ions start to bind with the porphyrins. Consequently, the change of colour is observed only at high adsorption level (around 800 mg/g), making the material inadequate for real-time mercury monitoring.

Therefore, cellulose-based adsorbents represent a more sustainable alternative, combining effective contaminant removal with lower environmental impact and greener synthesis routes.

3.2.4. Possible larger-scale applications of CNS: sediment remediation

Based on previous research conducted by O^{SCM} Lab, reported in Fiorati et al. [74],, adsorption tests in artificial sea water demonstrated that CNS exhibit remarkably high mercury adsorption capacities.

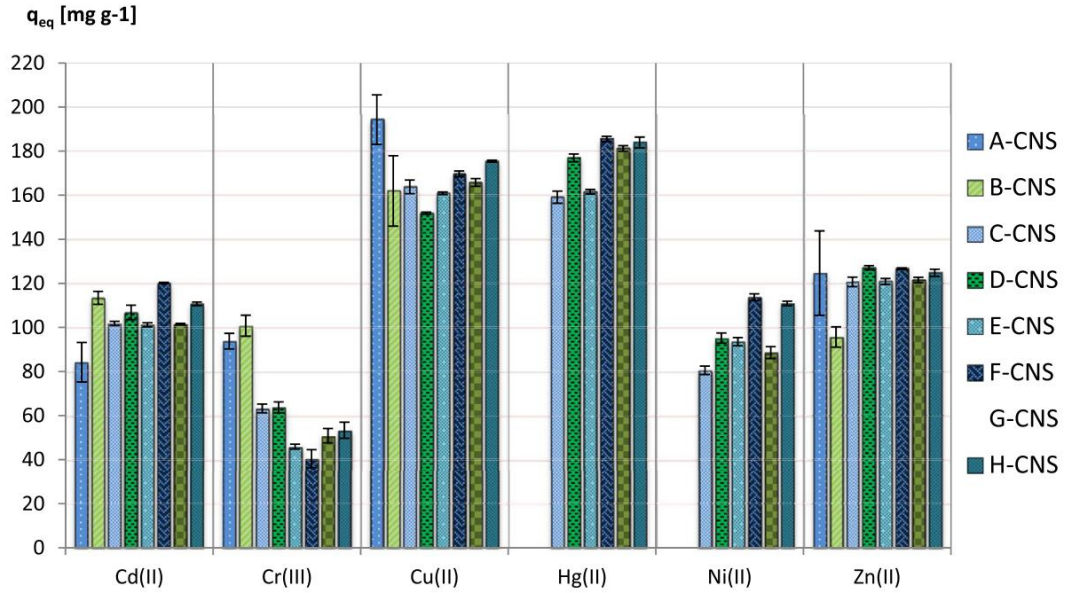

Figure 25: CNS adsorption capacity at the equilibrium for different metals [83]

Figure 25 illustrates the equilibrium adsorption capacities (q_{eq} [mg/g]) of different CNS samples toward six metal ions: Cd(II), Cr(III), Cu(II), Hg(II), Ni(II), and Zn(II) in sea water. The performance of the CNS variations for a particular ion is compared in each bar cluster. Specifically, the adsorption capacities of copper and mercury show the highest values, ranging from about 160 to 200 mg/g, indicating the significant potential of these materials. These results demonstrate the substantial potential of

cellulose-based nanomaterials as practical and effective options for emerging water treatment technology. [69]

These adsorption capacities in seawater are extremely high, supporting the positive evaluation of CNS for sediment remediation, as discussed in Section 1.5.1. However, the large quantity of CNS required for sediment capping represents a major limitation. Therefore, assessing the feasibility of industrial-scale production is essential, particularly in view of potential large-scale applications that would require substantial amounts of CNS. The scale-up strategy proposed in Section 3.2.4.2 is expected to help address this challenge.

This project is being conducted in collaboration with the University of Palermo (UniPa) and the University of Enna (UniKore).

The selected CNS formulation for sediment capping is 1:1:18. The incorporation of citric acid as a cross-linker is essential to minimize the amount of bPEI and limit its potential release, which has been reported to inhibit the growth rate of marine microalgae [36] [69].

The proposed approach involves the use of CNS as a capping material encapsulated between two layers of a geotextile fabric with an appropriate mesh. Similar techniques have already been reported in the literature [82]. The capping material was prepared by grinding the air-dried CNS in a mortar, obtaining a homogeneous powder.

Particle size analysis was performed to establish the selection of the appropriate geotextile material. The results, shown in Figure 26, indicate a bimodal distribution with two main peaks. The first peak corresponds to a fraction of smaller particles, whereas the second peak represents the predominant concentration of larger particles. The characteristic diameters indicate that 90% of all particles have a diameter below 594 µm.

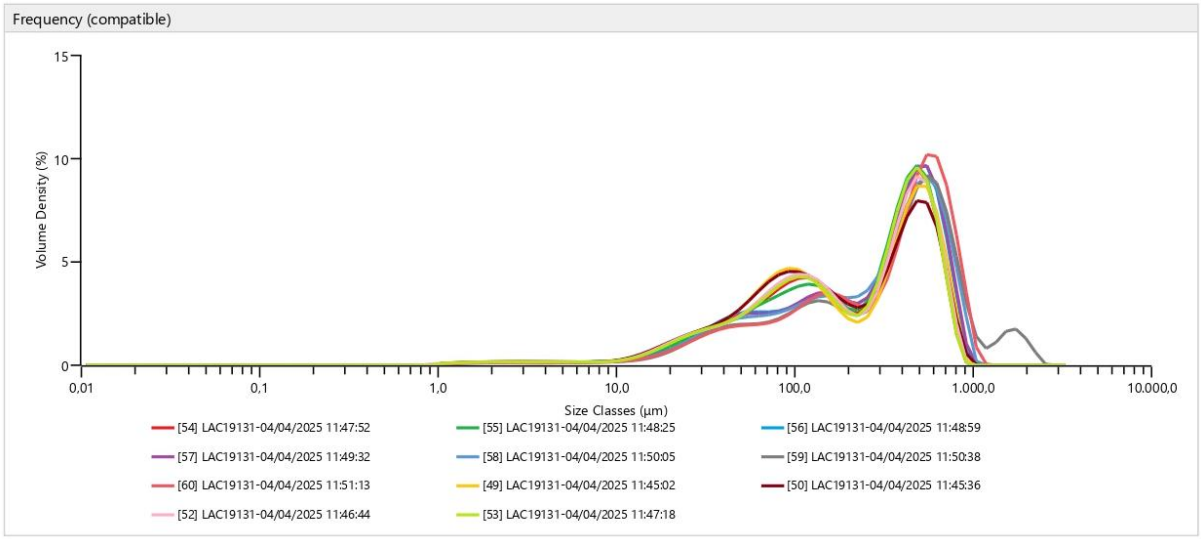

Figure 26: Particle size distribution

3.2.4.1. Literature Review

In this chapter, recent literature is examined and a possible scale-up strategy for TEMPO-mediated oxidation is discussed.

Paquin *et al.* [74] propose an interesting study, which develops the scale-up of TEMPO-mediated oxidation using ultrasound. They compare two systems: batch lab scale ultrasonic bath with a glass reactor and a semi-continuous flow-through sonoreactor.

Sonochemistry refers to a branch of chemistry that focuses on comprehending the effect of ultrasound in forming acoustic cavitation in liquids. The collapse of cavitation bubbles releases localized high energy, leading to the generation of reactive radical species that can initiate chemical reactions [75]. When cavitation bubbles burst, releasing energy, the reaction medium is broken down into numerous radical species, which are used as a reagent in chemistry. Several studies have demonstrated that acoustic cavitation significantly improves the efficiency of cellulose oxidation [76].

The equipment used are: a 45 L flow-through sonoreactor operated in semi-continuous mode, shown in Figure 27, and an ultrasonic bath combined with an ultrasonic generator operating at 170 kHz. The reagents ratios used are 0.1 mmol/g of 4-acetamino-TEMPO, 3.1 mmol/g of NaClO and 0.16 mmol/g of NaBr. Both reactions are conducted at 25°C for 90 min, with the pH maintained at 10 using an automated controller.

The sonochemical activity inside the sonoreactor is characterized using potassium iodide (KI) dosimetry. When ultrasound is applied to an aqueous solution of 0.1 M KI, the iodide ion is oxidized to iodine, which subsequently reacts with the excess of iodide ion to form tri-iodide ion [77]. The formation rate of iodide ion is an indirect measure of radical species generation resulting from the transient cavitation bubbles. This measure is used as a scaling parameter to scale-up the reaction conditions from the ultrasonic bath to the flow-through sonoreactor. The sonoreactor was calibrated using KI dosimetry after the iodide ion production rate was determined in the ultrasonic bath under ideal conditions. A linear correlation between the nominal input and the iodide ion formation rate is established and used to estimate the power required in the flow-through system.

Surprisingly, compared to the glass reactor, the flow-through sonoreactor needed about 98% less nominal input power to generate the same radical species production. This result clearly indicates the high efficiency of the sonotube configuration in promoting acoustic cavitation.

Moreover, when the oxidation is carried out in the sonoreactor, carboxylate groups formation increases by a factor of 2.6 compared to the glass reactor. This improvement is achieved with a reduction of input energy intensity of 87.5%. Overall, the flow-through sonoreactor (16.4 W/L) demonstrated a clear superiority over the ultrasonic

bath glass reactor (500 W/L), corresponding to a reduction of approximately 96.7% in applied energy density.

In conclusion, cellulose oxidation in the flow-through system resulted in lower energy consumption and a higher rate of carboxyl group formation under ultrasonic conditions. These findings clearly demonstrate the advantages of flow-through sonoreactor for efficient and scalable sonochemical oxidation processes.

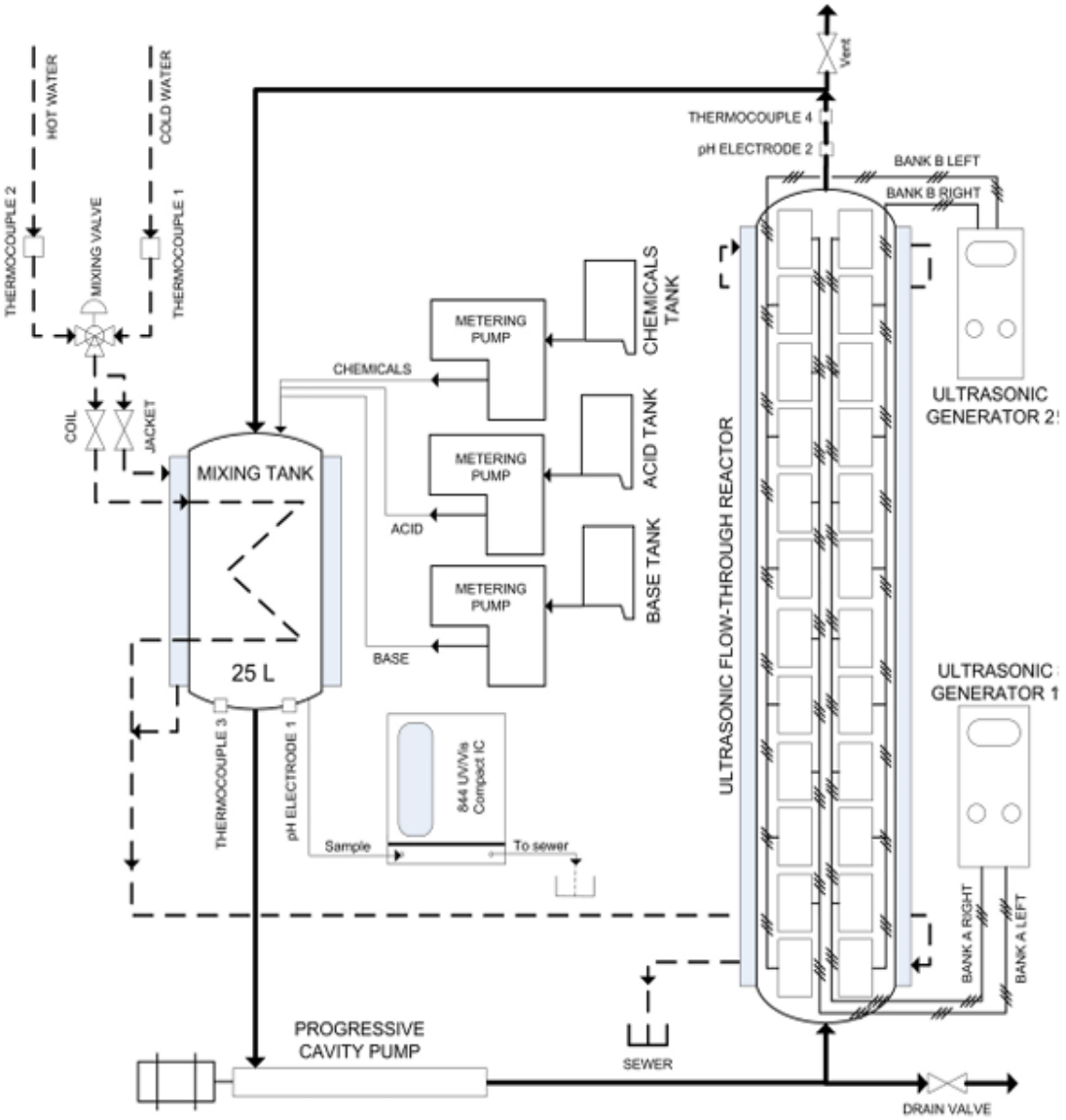

Figure 27: Schematic diagram of the large-scale flow through sonoreactor [74]

Sanchez-Salvador *et al.* [78] conducted a comparative study between different scale-up approaches. The technologies analysed were: a twin-screw extruder, a bakery kneader and a batch stirred reactor. In addition, they examined different types of lignocellulosic

materials, including softwood and hardwood species, non-woody plants and recycled cellulose.

The twin-screw extruder strategy is better explored in this study proposed by Sánchez-Salvador *et al.* [79]. This configuration enables simultaneous chemical oxidation and mechanical fibrillation of cellulose through intensive kneading. A schematic representation of the pilot-scale twin-screw extruder is shown in Figure 28.

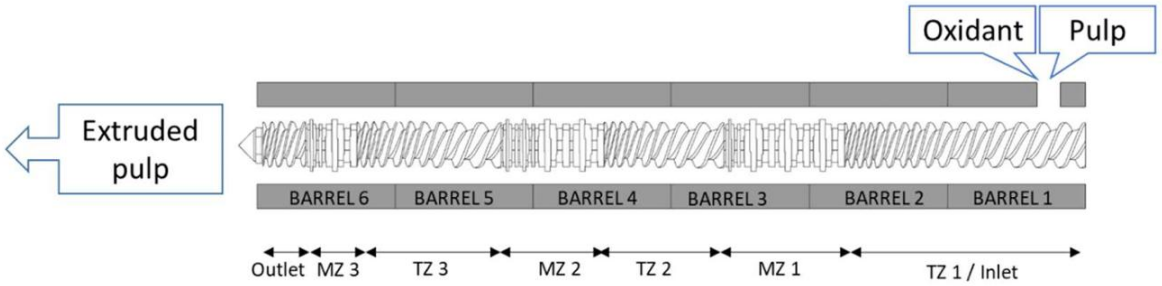

Figure 28: Pilot-plant twin-screw extruder configuration. TZ: transportation zone; MZ: mixing zone. [79]

Two distinct streams are used to introduce the reagents into the extruder. The first stream consists of cellulose pulp, that has been soaked in water for 24 h to promote fibres swelling and subsequently disintegrated using a PTI pulp disintegrator, together with a pH buffer solution. On the other hand, the oxidant stream is composed of TEMPO, NaBr and NaClO solution (7wt%), all stirred until complete dissolution.

The twin-screw extruder's speed has been set at 100 rpm to prevent clogging, resulting in a residence time of approximately 125 seconds per step. The temperature inside the extruder is between 23 and 28°C, trying to avoid any possible local hotspots due to the high pressure. The addition of the pH buffer allows to maintain the pH around 9.5-10 to favour the oxidation reaction.

After exiting the extruder, the oxidized fibres are washed and filtered. Cellulose nanofibers are subsequently produced from the filtered oxidized pulp using a laboratory-scale homogenizer.

To quantify the extent of oxidation happening during the TSE process, a fraction of the oxidized pulps is immediately immersed in water upon exiting the extruder to quench the reaction, followed by washing and filtering (OPs-0). The remaining fraction is left in contact with the reaction medium for an additional 4 h prior to washing and filtration (OPs-4). A nylon mesh is used for vacuum filtration, and then the pulp is repeatedly washed until the pH is neutral.

The results shows higher oxidant consumption in OPs-4, indicating that the oxidation reaction continues after extrusion if the reaction medium is not promptly removed.

The study investigates the impact of many extrusion steps and various ratios between the two feed streams. A higher degree of oxidation and more carboxyl groups production resulted from increasing the number of stages, which improved cellulose

accessibility. A production rate of 527 g of dry oxidized pulp per hour is obtained with a single extrusion phase, representing a significant improvement compared to conventional stirred reactors. However, the total yield of oxidized pulp decreases to around 150 g of dry oxidized pulp per hour as the number of extrusion operations increases.

The bakery kneader procedure is better investigated in another paper by Sanchez-Salvador [80]. The TEMPO-mediated oxidation is conducted using 0.025 mmol of TEMPO, 0.5 mmol of NaBr and 2.5 mmol of NaClO per gram of pulp. The temperature is kept around 25 °C and the pH was adjusted between 9.5-10.5, using 2 M NaOH. To avoid any mixing limitations, the pulp concentration is 100 g of pulp/L despite the higher capacity.

Initially, the pulp and the pH buffer are kneaded for one minute, after which the catalysts is added and further kneaded. The reaction is initiated by the addition of NaClO solution. After 10 minutes, the oxidation is considered complete, thus the oxidized pulp is subsequently filtered and washed until pH neutrality. The cellulose nanofibrils are then produced using a high-pressure homogenization.

Due to the high pulp concentration in the bakery kneader, the reaction time is remarkably reduced to 10 minutes. In fact, the high concentration of reagents simplifies the interaction between them, making the reaction faster. However, the formation of carboxylic groups reaches 0.84 mmol/g, a lower value than the theoretical one of 1 mmol/g based on the reagents ratio.

An additional advantage of the bakery kneader is the production volume for the low volume required. In fact, for a 10 L reactor, around 500 g of oxidized pulp is produced.

As well, in the batch stirred reactor, the reaction conditions are the same. The reagents ratio is fixed at 0.025 mmol of TEMPO, 0.5 mmol of NaBr and 2.5 mmol of NaClO per gram of pulp. The pulp concentration is set at 30 g/L, to avoid any agitation limitation. The reaction time is established at 30 minutes to ensure complete oxidation, adjusting the pH at 10 for the whole time. In the end, the oxidized pulp is filtered and washed until pH neutrality. Again, cellulose nanofibrils are produced using a high-pressure homogenization.

To evaluate the results of the batch stirred reactor, the experimental data reported in reference [80] are used. The carboxylic content reaches around 1.00 mmol/g of pulp. In the first minutes of the reaction, the oxidant mostly converts the hydroxy groups to carboxylic ones. However, as time passes, cellulose oxidation becomes minimal and NaClO attacks the β-glycosidic bond of the cellulose, leading to depolymerization. [81]

Comparing these three technologies, it is possible to notice that the reagent consumption and the operating conditions are nearly constant. However, the output pulp concentrations extremely change. The outlet pulp concentrations are: 116-150 g/L

for the twin-screw extruder, 82-96 g/L for the 10 L bakery kneader and 24-28 g/L for the stirred batch reactor. This is reflected on the oxidized pulp production. In the twin-screw extruder, it changes depending on the number of extruder passes, ranging from 120 to 500 g of oxidized pulp per hour. In the 10 L bakery kneader, the oxidized pulp production is around 550 grams per hour. In the stirred batch reactor, it is around 100 g/h. This demonstrates that the higher the pulp concentration, the more the oxidized pulp production, indicating that scaling up the oxidation process significantly enhances productivity and process continuity.

Regarding the carboxylic content, it is slightly higher (until 10%) in the kneader reactor with respect to the stirred batch reactor, due to the effective kneading. Instead, the twin-screw extruder with multiple passes shows an increased number of carboxylic moieties compared to the one-step configuration, demonstrating enhanced oxidation efficiency due to increased cellulose accessibility.

These studies [78], [79], [80], [81] illustrate that the kneader reactor and the one-pass twin-screw extruder have the higher oxidized pulp production. The twin-screw extruder allows continuous and high consistency operation while the kneader reactor has longer times and discontinuous operation.

3.2.4.2. Possible scale-up strategy

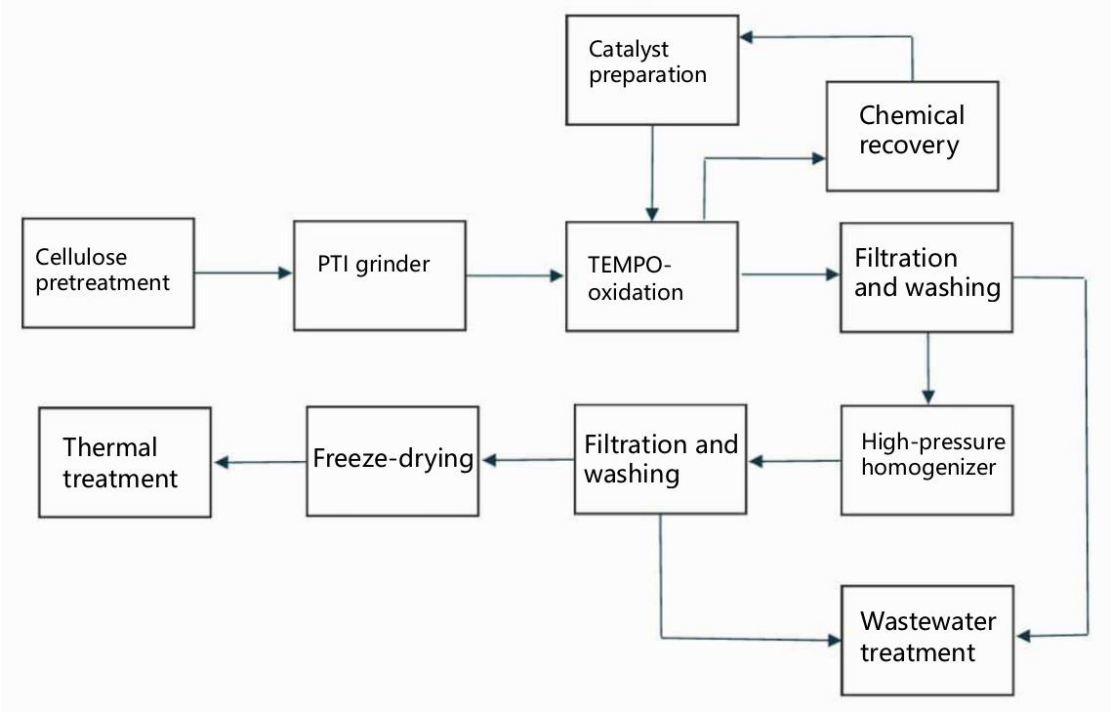

Figure 29: Process Flow Diagram (PFD) of a possible plant for CNS production

Figure 29 represents a possible representation of a plant for CNS production. The unit operations are discussed in the following sections.

The process begins with cellulose pre-treatment, where it is immersed in water to allow fibre swelling and improve chemical accessibility. The pre-treated cellulose is subsequently disintegrated using a pulp grinder, which mechanically disintegrate the fibers to increase the available surface area.

In parallel, the catalyst solution is prepared, dissolving TEMPO, KBr in aqueous solution.

As analysed in 3.2.4.1, there are different possibility for the choice of the TEMPO-mediated oxidation reactor. The use of a twin-screw extruder enables continuous operation, allowing higher production efficiency compared to conventional batch reactors, which are typically employed in industry. Additionally, batch reactors require careful control to ensure homogeneous mixing throughout the reaction medium. For these reasons, a twin-screw extruder has been selected as the reactor for this process.

The disintegrated pulp is fed into the reactor with the catalyst solution. To maintain the pH above 10, a pH buffer is added into the cellulose suspension.

After the reaction has finished, the reaction mixture undergoes washing and filtration, which removes residual reagents, salts, and by-products while isolating the oxidized cellulose. For this passage, a belt filter (Figure 30) is selected. The TEMPO-oxidized cellulose slurry is fed to a continuously moving horizontal belt. A vacuum system, located below the belt, draws the liquid through the filter belt while forming a solid cake on the filter belt. The cake can be washed multiple times. After the deliquoring zone, the cake is discharged.

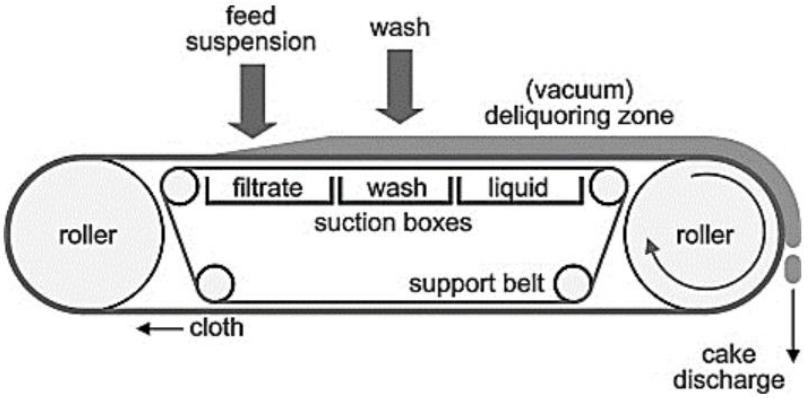

Figure 30: Belt Filter Design [87]

A rotary vacuum drum filter can also be employed, but it provides a lower washing efficiency and tends to produce a more compact filter cake. In contrast, a belt filter allows the integration of multiple washing stages along the filtration path, which is fundamental to eliminate all the unreacted reagents. Furthermore, belt filters offer

greater operational flexibility, allowing better control over residence time and filter cake thickness.

Finally, the purified oxidized cellulose is processed using a high-pressure homogenizer. This mechanical treatment fibrillates the oxidized fibres, producing TOCNF with enhanced surface area and functional properties.

As previously mentioned, TOCNF are washed and filtered in a belt filter.

To synthesize the CNS, TOCNF and the crosslinkers are mixed in a stirred batch reactor. The mixture is placed in molds, without any particular shape. They are frozen in a separate freezer and subsequently, put in the lyophilizer. The pre-freezing is a better choice with respect to the freezing inside the lyophilizer because allows a better control on the freezing velocity and on the CNS microstructure [82]. Moreover, the lyophilization is time- and energy- intensive unit operation and if only used for the sublimation and desorption phases, the productivity is optimized [83].

Therefore, a freezer room is selected to freeze the CNS sample at approximately -15 to -20°C, ensuring a moderate and controlled freezing velocity. Subsequently, the CNS are subjected to lyophilization (Figure 31).

Figure 31: Industrial lyophilizer [88]

To perform the thermal treatment mentioned in **Errore. L'origine riferimento non è stata trovata.**, a tray batch oven or forced ventilation oven are the best option. Both machines can be programmed to do a controlled temperature ramps and the forced air circulation guarantees a homogeneous temperature inside the chamber. Due to the long-time residence time of the last step, a conveyor oven is not recommended. The necessary conveyor length would result in an impractical and excessively large equipment.

All the auxiliary equipment such as storage tanks, pumps, wastewater treatment system and controlling system have not been considered but are necessary for the safe operation of the plant.

Possible improvements will be discussed below:

- Multiple tanks can be introduced to make the swelling stage continuous. Each tank is filled with cellulose and water to initiate the swelling. The tank can be designed to supply the material required while another batch of cellulose undergoes swelling. This configuration allows continuous operation of the overall process.
- The reaction medium can be recycled to avoid further waste and use of chemicals. Xu *et al.* [84] proposed reusing of 50-80% of filtrated medium and adding 20-50% of fresh catalysts. TEMPO was recovered by extraction with ethyl acetate and then distilled. Although this recycling approach resulted in a longer oxidation time, the properties of the TEMPO-oxidized cellulose were preserved.
  Another approach is proposed by Serra *et al.* [85], which consists of reducing the amount of TEMPO used in the reaction. Their research demonstrates that reducing the amount of TEMPO by 50% does not affect the reaction time or the chemical and physical properties of the oxidized fibers. This strategy not only lowers the consumption of chemical reagents but also contributes to a reduction in overall process costs.
- Another important improvement is the recovery of the water used to wash the products, since it is a substantial volume. In particular, the water from the initial washes after oxidation contains unreacted chemicals, which can be recovered through electrolysis and solid extraction [86].

3.3. PFAS

To extend the investigation to aquatic contaminants other than mercury, the SiTTC porphyrinic molecule was considered, as it has been previously reported in Section 1.5.2 to be sensitive to fluorine in aqueous environments.

The aim of this part of the work was to incorporate SiTTC into the CNS matrix for the recognition of PFAS. The functionalized nanosponges were synthesized as described in Section 2.1.5, morphologically characterized by SEM analysis, and subsequently evaluated through colorimetric tests. PFOA was selected as a model PFAS compound to assess the sensing capability.

3.3.1. SEM analysis

The CNS modified with SiTTC were analysed through SEM analysis to evaluate the morphology and the porosity. For each sample, the inner and external sides were examined. Only one CNS for each batch was analysed, assuming minimal differences between all the samples. Additionally, to observe the internal structure, the samples

were sectioned by applying mechanical pressure, which may have altered the initial morphology of the sponges.

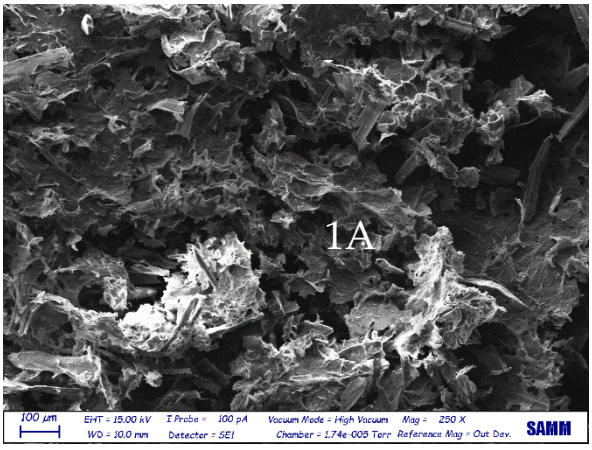

Internal side LDV 8

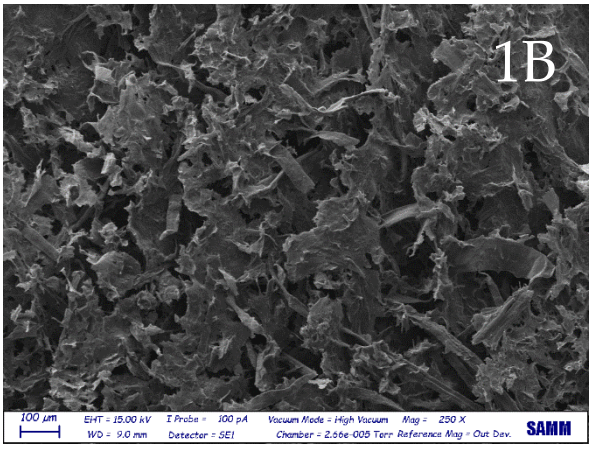

External side LDV 8

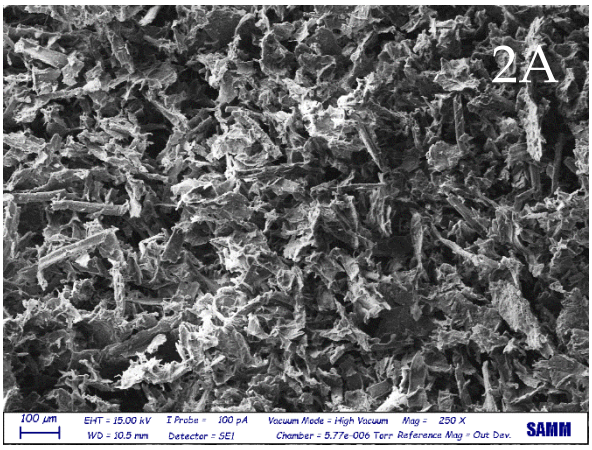

Internal side LDV 44

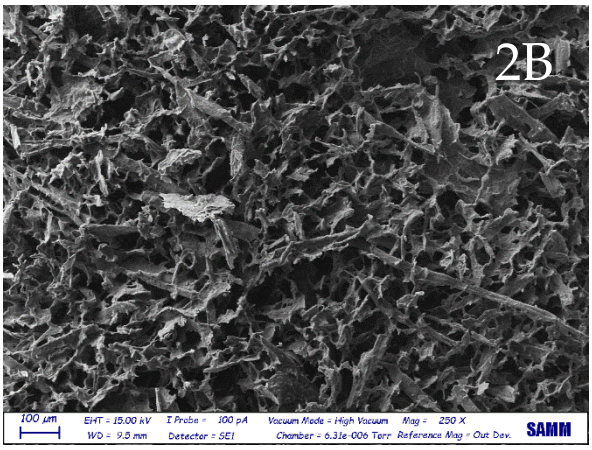

External side LDV 44

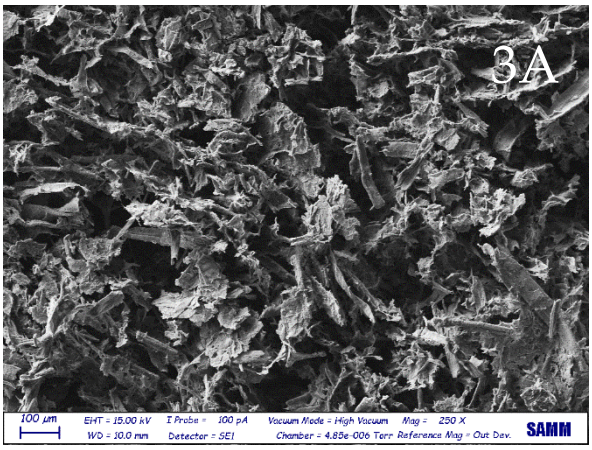

Internal side LDV 45

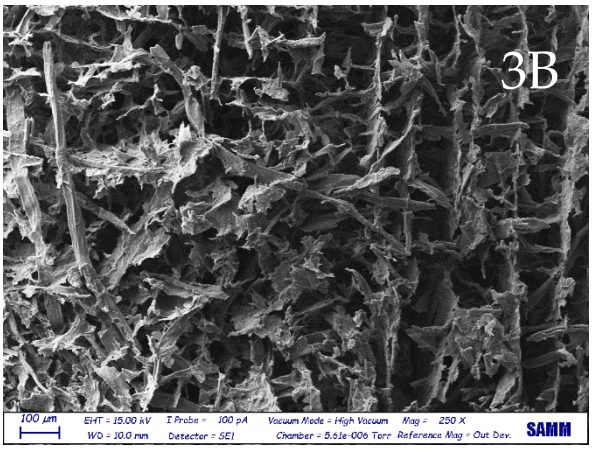

External side LDV 45

Figure 32: SEM analysis of SiTTC-functionalized CNS

In 1A and 1B of Figure 32, LDV8 is presented. The sponge is cross-linked using PEG with 8 arms, which is a notable difference compared to other sponges synthesized with bPEI. The structure appears composed of aggregated fibers forming irregular cavities and channels. The morphology seems rough, fractured and jagged. The pore architecture appears irregular, with elongated cavities likely generated by ice crystal growth during the freezing step. Overall, the morphology confirms the formation of a porous structure, suitable to diffuse contaminants inside it.

In 2A and 2B, the sample shown is LDV44, synthesized with bPEI 25 kDa. Compared to LDV8, this structure appears more porous. While some regions remain jagged and irregular, the material exhibits a more interconnected network. The internal surface of the CNS appears more fragmented and heterogeneous, with numerous sharp edges indicating that the surface may have been affected by mechanical separation.

The 3A and 3Bshow LDV45, synthesized with bPEI 1.8 kDa. The structure is more porous than LDV8 but less than LDV44. The sponge exhibits a heterogeneous morphology, with a combination of irregular rod-like structures and smaller fibrous aggregates, suggesting localized stress during freeze-drying or mechanical processing. The pore size distribution remains variable, with both small and moderately large cavities, which may facilitate selective diffusion and adsorption of molecules.

The differences in morphology between the samples can be attributed primarily to the molecular weight of the cross-linkers, which affects pore sizes and fiber aggregation.

The porosity of the sponges is calculated as area fraction, using the software ImageJ. The results are shown in Table 7.

CNS	Magnitude	Scale [μm]	Internal porosity	External porosity
LDV 8	250X	100	20.32% (2)	31.91% (2)
	500X	20	22.84% (3)	28.27% (3)
	250X	100	17.66% (5)	30.22% (5)
	500X	20	18.99% (6)	29.06% (6)
LDV 44	250X	100	31.64% (2)	26.33% (2)
	500X	20	26.76% (3)	26.79% (3)
	250X	100	29.38% (5)	26.78% (5)
	500X	20	30.01% (6)	24.21% (6)
LDV 45	250X	100	27.59% (2)	26.25% (2)
	500X	20	29.96% (3)	23.07% (3)
	250X	100	30.93% (5)	27.94% (5)
	500X	20	25.91% (6)	30.37% (6)

Table 7: SEM analysis of SiTTC-functionalized CNS

As in 3.2.2.1, the difference between internal and external porosity can be explained by analysing the freeze-drying process or by an altered morphology due to the sectioning. The external layer's high porosity allows contaminants to penetrate and diffuse more quickly, while the inner region's smaller pores enhance the structural stability.

The different porosity of LDV8, observed in the SEM images, is confirmed by the porosity calculated through ImageJ.

3.3.2. Colorimetric detection test

To evaluate the colorimetric response of the SiTTC-functionalized CNS, a series of preliminary tests were conducted as described in section 2.3.

All tests were performed in PBS solution to avoid unwanted colour changes due to changes in the pH of the solution when the PFOA was added..

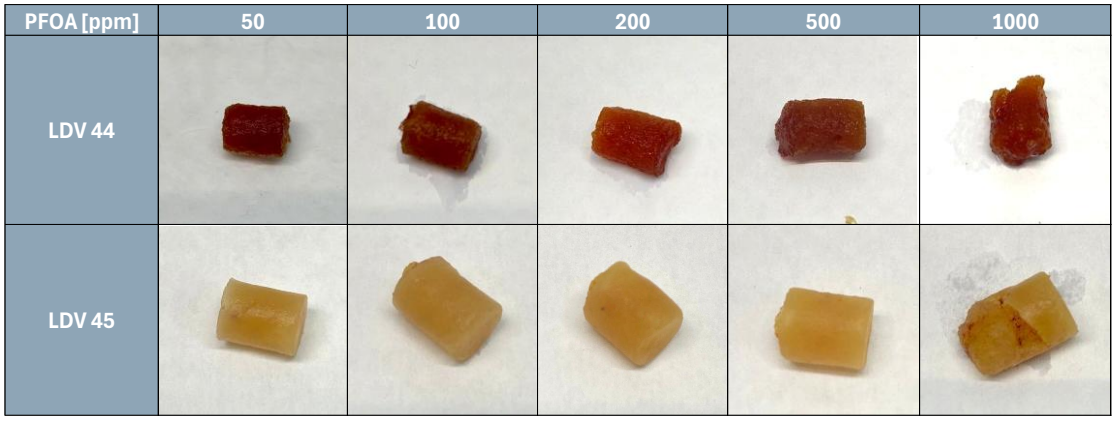

Figure 33: SiTTC-functionalized CNS's colorimetric tests

Figure 33 shows the CNS samples in PFOA–PBS solution after 24 hours under shaking conditions. In LDV44, a clear colorimetric response is observed, with a slight but noticeable variation in colour as a function of PFOA concentration. Moreover, the three-dimensional structure of the CNS is preserved, with no visible damage.

In contrast, LDV45 does not exhibit any colorimetric response. The differences between the two batches are not solely attributable to the cross-linker, bPEI 25 kDa for LDV44 and bPEI 1.8 kDa for LDV45, but also to the use of two distinct sensor batches. Specifically, LDV45 was prepared with a newly synthesized batch of Si-TTC, as the previous one had been depleted.In particular, variations in the hydration degree of the sensor may have influenced the weighing step, potentially leading to an underestimation of the actual amount of active compound and, consequently, to an altered or absent response.In fact, as shown in Figure 34, an old batch of LDV45 tested in 200 ppm of PFOA in PBS solution presents a pronounced colorimetric response, thereby confirming problem with the new batch.

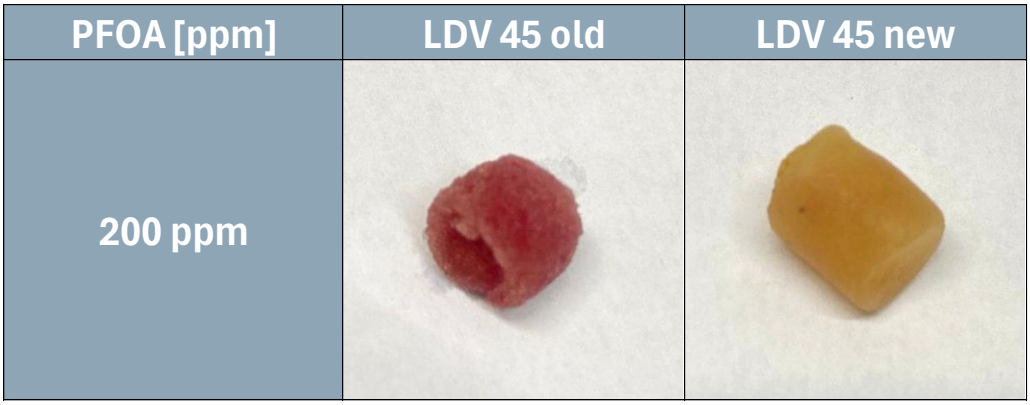

Figure 34: Comparison between LDV45 old and new batches

A slight yellowing of the solutions was observed during the colorimetric tests, possibly attributable to minor bPEI leaching. The functionalized CNS were not subjected to

post-synthesis washing, as this step can induce shrinkage phenomena and partial collapse of the three-dimensional porous structure, as previously observed in the thesis of Davide Luzzini [70]. A possible solution to prevent bPEI leakage is the introduction of a co-crosslinker, such as citric acid, as previously implemented in the 1:1:18 formulation [89].

4 Conclusion and future developments

In this experimental thesis, the successful synthesis of sustainable smart materials capable of both adsorbing and detecting water contaminants was achieved. CNS were prepared from renewable and environmentally friendly components, highlighting their strong potential for environmental remediation. Morphological characterization by scanning electron microscopy confirmed the formation of a highly porous three-dimensional network able to trap pollutants, and demonstrated that structural modifications, such as functionalization of different building blocks and the introduction of spacers, significantly influence material porosity.

A key outcome of this work is that the incorporation of different porphyrinic sensors (e.g., TPPS4, TPPCH2 and Si-TTC) enables CNS to detect mercury ions and PFAS through a clear colorimetric response, coupling sensing with adsorption. Importantly, alternative functionalization routes were successfully explored, showing that the sensing functionality can be introduced not only through bPEI but also directly within the cellulose backbone. The proposed functionalization strategies exhibited a high degree of modification, which is essential for the effective incorporation of porphyrinic molecules. CNS prepared from TOCNF-APTES and further functionalized with TPPCH2 will be optimized and subjected to adsorption studies, while analogous adsorption and detection investigations will be performed on CNS obtained from cellulose modified with 1,8-diaminooctane.

Despite these advances, further improvements are required. Future work will focus on incorporating additional porphyrins, including TPPS4 and Si-TTC, directly into the cellulose matrix, requiring the development of efficient and selective functionalization strategies. Adsorption and sensing performance toward PFAS can be further optimized by exploring new formulations of CNS, including the use of co-crosslinkers (e.g. citric acid, currently present in CNS not functionalized with porphyrins).

Finally, scale-up studies demonstrated that both TOCNF production and the subsequent fabrication of CNS are scalable, supporting their use in applications requiring large material volumes, such as sediment remediation. The material has already shown adsorption capability in seawater, and the development of effective in situ sediment-coating systems represents a promising research direction. Overall, the scalability of the proposed approach strengthens the feasibility of translating CNS-based technologies from laboratory research to real environmental applications.

5 References

[1] "ONU," [Online]. Available: https://unric.org/it/agenda-2030/.

[2] H. Ali , E. Khan and I. Ilahi, "Environmental Chemistry and Ecotoxicology of Hazardous Heavy Metlas: Environmental Persistence, Toxicity, and Bioaccumulation," *Journal of Chemistry* , 2019.

[3] "Minamata Convention on Mercury," [Online]. Available: https://minamataconvention.org/en.

[4] UNEP, Global Mercury Assessment 2018, 2018.

[5] M. UNEP, State of the Mediterranean Marine and Coastal Environment, 2012.

[6] EEA, Mercury in Europe's Environment: A priority for European and global action, 2018.

[7] Z. Abunada, M. Alazaiza and M. Bashir, "An Overview of Per- and Polyfluoroalkyl Substances (PFAS) in the Environment: Source, Fate, Risk and Regulations," *Water,* 2020.

[8] M. Mastrantonio , E. Bai , R. Uccelli , V. Cordiano, A. Screpanti and P. Crosignani, "Drinking water contamination from perfluoroalkyl substances (PFAS): an ecological mortality study in the Veneto Region, Italy," *The European Journal of Public Health* , 2017.

[9] D. Cossa, J. Knoery, D. Banaru and e. al., "Mediterranean Mercury Assessment 2022: An Updated Budget, Health Consequences, and Research Perspectives".

[10] B. R.A., "Mercury Toxicity and Treatment: A Review of the Literature," *Journal of Environmental and Public Health,* 2012.

[11] M. Balali-Mood, K. Nasseri, Z. Tahergorabi and al., "Toxic Mechanisms of Five Heavy Metals: Mercury, Lead, Chromium, Cadmium, and Arsenic," *Frontiers in Pharmacology,* 2021.

[12] EEA, "Heavy Metal Emissions in Europe," [Online].

[13] N. Selin, "Global Biogeochemical Cycling of Mercury: A Review," *Annual Review of Environment and Resources,* 2009.

[14] W.-M. L. C. J. Rothenberg S.E, "Rice methylmercury exposure and mitigation: A comprehensive review," *Elsevier,* 2014.

[15] L. Wang, D. Hou, Y. Cao and e. al., "Remediation of mercury contaminated soil, water and air: A review of emerging materials and innovative technologies," *Environment International,* 2020.

[16] D. Teng, K. Mao, W. Ali and e. al., "Describing the toxicity and sources and the remediation technologies for mercury-contaminated soil," *RSC Advances,* 2020.

[17] D. Veeraswamy, A. Subramanian, D. Mohan and e. al., "Exploring the origins and cleanup of mercury contamination: a comprehensive review," 2023.

[18] J. Georgin, D. Franco, Y. Dehmani and e. al., "Current status of advancement in remediation technologies for the toxic metal mercury in the environment: A critical review," *Science of the Total Environment,* 2024.

[19] M. S. Ray D., "Sources, toxicity, and remediation of mercury: an essence review," *Springer Nature Switzerland ,* 2019.

[20] I. Ahmad, N. Fatima, E. Naz and e. al., "Treatment Methods for Mercury Removal From Soil and Wastewater," 2024.

[21] L. Ding, X. Luo, P. Shao and e. al., "Thiol-Functionalized Zr-Based Metal Organic Framework for Capture of Hg(II) through a Proton Exchange Reaction," *ACS Sustainable Chemistry & Engineering,* 2018.

[22] M. Dehgani, M. Aghaei and P. Barshardoust, "An insight into the environmental and human health impacts of per- and polyfluoroalkyl substances (PFAS): exploring exposure pathways and their implications," *Environmental Sciences Europe ,* 2025.

[23] E. Panieri, K. Baralic, D. Djukic-Cosic and L. Saso, "PFAS Molecules: A Major Concern for the Human Health and the Environment," *Toxics,* 2022.

[24] E. Dobrzynska, P. Wasilewski and M. Posniak, "Per- and Polyfluoroalkyl Substances (PFASs): A Comprehensive Review of Environmental Distribution, Health Impacts and Regulatory Landscape," *Applied Sciences* , 2025.

[25] A. Anik, I. Aurnab and M. Sultan, "A State-of-Art review of the Environmental Mixtures, Exposure, and Health Risks of PFAS: A Special Focus on Developing Country," *Water Air Soil Pollution* , 2025.

[26] R. Buck, J. Franklin, U. Bergen, J. Conder and e. al., "Perfluoroalkyl and Polyfluoroalkyl Substances in the Environment: Terminology, Classification and Origins," *Integrated Enviromentla Assessment and Management* , vol. 7, no. 4, 2011.

[27] S. Wee and A. Arin, "Environmental impacts, exposure pathways, and health effects of PFOA and PFOS," *Ecotoxicology and Environmental Safety* , 2023.

[28] H. Zhang, H. Xu and B. Qin, "Review on the sources, distribution and treatment of per- and polyfluoroalkyl substances in global groundwater," *Environmental Research* , 2025.

[29] S. Fenton, A. Ducatman, A. Boobis, J. DeWitt and e. al., "Per- and Polyfluoroalkyl Substance Toxicity and Human Health Review: Curretn State of Knowledge and Strategies for Informing Future Research," *Environmental Toxicology and Chemistry* , vol. 00, no. 00, pp. 1-25, 2020.

[30] V. Gallo , G. Leonardi , B. Genser, M.-J. Lopez-Espinosa , S. Frisbee, L. Karlsson , A. Ducatman and T. Fletcher , "Serum Perfluoroocatanoate (PFOA) and Perfluorooctane Sulfonate (PFOS) Concentrations and Liver Function Biomarkers in a Population with Elevated PFOA Exposure," *Environmental Health Perspectives* , vol. 120, no. 5, 2012.

[31] R. Lewis , L. Johns and J. Meeker , "Serum Biomarkers of exposure to Perfluoroalkyl Substances in Relation to Serum Testosterone and Measures of Thyroid Function among Adults and Adolescents from NHANES 2011-2012," *Environmental Research and Public Health* , 2015.

[32] G. Post , P. Cohn and K. Cooper, "Perfluorooctanoic acid (PFOA), an emerging drinking water contaminant: A critical review of recent literature," *Environmental Research,* 2012.

[33] R. Amen , A. Ibrahim , W. Shafqat and E. B. Hassan , "A Critical Review on PFAS Removal from Water: Removal Mechanism and Future Challenges," *Sustainability* , 2023.

[34] D. Wanninayake, "Comparison of currently available PFAS remediation technologies in water: A review," *Journal of Environmental Management* , 2021.

[35] E. Marihno, "Cellulose: A comprehensive review of its properties and applications," *Sustainable Chemistry for the Environment,* 2025.

[36] L. Riva , A. Fiorati and C. Punta, "Synthesis and Application of Cellulose-Polyethyleimine Composites and Nanocomposites: A Concise Review," *Materials,* 2021.

[37] B. Thomas, M. Raj, J. Joy and e. al., "Nanocellulose, a Versatile Green Platform: From Biosources to Materials and Their Applications," *Chemical Reviews,* 2018.

[38] A. Balea, A. Blanco, M. Delgado-Aguilar and al., "Nanocellulose Characterization Challenges," *BioResources,* 2021.

[39] S. A. Jose, N. Cowan, M. Davidson and e. al., "A Comprehensive Reviw on Cellulose Nanofibers, Nanomaterilas and Composites: Manufacturing, Properties, and Applications," *Nanomaterials,* 2025.

[40] L. Melone, B. Rossi, N. Pastori and e. al., "TEMPO-Oxidized Cellulose Cross-Linked with Branched Polyethyleneimine: Nanostructured Adsorbent Sponges for Water Remediation," *ChemPlusChem,* 2015.

[41] M. Ateia , M. Attia , A. Maroli , N. Tharayil , F. Alexis, D. Whitehead and T. Karanfil , "Rapid Removal of Poly- and Perfluorinated Alkyl Subatances by Poly(ethylenimine)-Functionalized Cellulose Microcrystals at Environmentally Relevant Conditions," *Environmental Science and Technology Letters* , vol. 5, pp. 764-769, 2018.

[42] B.-W. Gu, C.-G. Lee, T.-G. Lee and S.-J. Park, "Evaluation of sediment capping with activated carbon and nonwoven fabric mat to interrupt nutrient release from lake sediments," *Science of the Total Environment* , 2017.

[43] D. Mussabek , L. Ahrens, K. Persson and R. Berndtsson , "Temporal trends and sediment-water partitioning of per- and polyfluoroalkyl substances (PFAS) in lake sediment," *Chemosphere* , 2019.

[44] Q. Yang, Y. Wang and H. Zhong , "Remediation of mercury-contaminated soils and sediments using biochar: a critical review," *Biochar*, 2021.

[45] J. Wikstrom, S. Bonaglia, R. Ramo, G. Renman, J. Walve and e. al., "Sediment Remediation with New Composite Sorbent Amendments to Sequester Phosphorus, Organic Contaminants and Metals," *Environmental Science and Technology* , 2021.

[46] F. Caroleo, G. Magna, C. Damiano and e. al., "Colour Catcher sheet beyond the laundry: a low-cost support for realizing porphyrin-based mercury ion sensors," *Sensors and Actuators: B. Chemical* , 2022.

[47] X. Liu , M. Tao and W. Zhang , "A highly selective and sensitive recyclable colorimetric Hg2+ sensor based on the porphyrin-functionalized polyacrylonitrile fiber," *Journal of Materials Chemistry A*, 2015.

[48] M. Rezazadeh, S. Seidi, M. Lid, S. Pedersen-Bjergaard and Y. Yamini, "The modern role of smartphone in analytical chemistry," *Trends in Analytical Chemistry* , 2019.

[49] L. F. Capitan-Vallvey, N. Lopez-Ruiz, A. Martinez-Olmos, M. Erenas and A. Palma, "Recent developments in computer vision-based analytical chemistry: A tutorial review," *Analytica Chimica Acta*, 2015.

[50] R. Paolesse , S. Nardis, D. Monti, M. Stefanelli and C. Di Natale, Porphyrinoids for Chemical Sensor Applications, 2017.

[51] Y. Ding , W.-H. Zhu and Y. Xie, Development of Ion Chemosensors Based on Porphyrin Analogues, 2017.

[52] E. Ahmadi, A. Ramazani, Z. Hamdi, A. Mashhadi-Malekzadeh and Z. Mohamadnia, "5,10,15,20-tetrakis(4-carboxylphenyl)porphyrin Covalently Bound to Nano-silica Surface: Preparation, Characterization and Chemosensor Application to Detect," *Silicon* , 2015.

[53] A. Adler, F. Longo, J. Finarelli , J. Goldmacher, J. Assour and L. Korsakoff, "A simplified synthesis for meso-tetraphenylporphine," *J Org Chem* , vol. 32, no. 2, pp. 476-476, 1967.

[54] R. Johnstone and e. al., "New Procedures for the Synthesis and Analysis of 5,10,15,20-Tetrakis(sulphophenyl)porphyrins and Derivatives through Chlorosulphonation," *Heterocycles*, vol. 43, no. 4, p. 829, 1996.

[55] G. Pomarico, D. Monti, M. Bischetti, A. Savoldelli and e. al., "Silicon(IV) Corroles," *Chemistry: A European Journal* , vol. 24, pp. 8438-8446, 2018.

[56] A. Isogai, T. Saito and H. Fukuzumi, "TEMPO-oxidized cellulose nanofibers," *Nanoscale* , 2011.

[57] S. Arfelis , R. Aguado and D. Civancik, "Sustainability of cellulose micro-/nanofibers: A comparative life cycle assessment of pathway technologies," *Science of the Total Environment* , 2023.

[58] Z. Tang, W. Li, X. Lin , Q. Miao, L. Huang, L. Chen and H. Wu, "TEMPO-oxidized Cellulose with High Degree of Oxidation," *Polymers* , 2017 .

[59] N. Masruchin and B.-D. Park, "Manipulation of Surface Carboxyl Content on TEMPO-Oxidized Cellulose Fibrils," *Journal of the Korean Wood Scienve and Technology* , vol. 43, no. 5, pp. 613-627, 2015.

[60] T. Rusconi , L. Riva , C. Punta , M. Solé and I. Corsi , "Environmental safety of nanocellulsoe: an acute in vivo study with marine mussels Mytilus galloprovincialis," *Environmental Science: Nano,* vol. 11, pp. 61-77, 2024.

[61] H. Khanjanzadeh, R. Behrooz, N. Bahramifar and e. al., "Surface chemical functionalization of cellulose nanocrystals by 3-aminopropyltriethoxysilane," *International Journal of Biological Macromolecules* , 2017.

[62] P. Zhang, Y. Lu, M. Fan, P. Jiang and Y. Dong, "Modified cellulose nanocrystals enhancement to mechanical properties and water resistance of vegetable oil-based waterborne polyurethane," *Applied Polymer Science* , 2019.

[63] F. Ludovici, R. Hartmann and H. Liimatainen, "Aqueous bifunctionalization of cellulose nanocrystals through amino and alkyl silylation: functionalization, characterization, and performance of nanocrystals in quartz microflotation," *Springer Nature,* 2022.

[64] M. Sun, H. Wang and X. Li, "Modification of cellulsoe microfibers by polyglutamic acid and mesoporous silica nanoparticles for Enterovirus 71 adsorption," *Materials Letters* , 2020.

[65] N. Ural , "The significance of scanning electron microscopy (SEM) analysis on the microstructure of improved clay: An overview," *Open Geosciences,* vol. 13, pp. 197-218, 2021.

[66] E. Frackowiak, A. Platek-Mielczarek, J. Piwek and K. Fic, "Advanced characterization techniques for electrochemical capacitors," in *Advances in Inorganic Chemistry* , 2022, pp. 151-207.

[67] "XRF scientific," [Online]. Available: https://www.xrfscientific.com/what-is-icp-spectroscopy/.

[68] S. Glassford, B. Byrne and S. Kazarian, "Recent applications of ATR FTIR spectroscopy and imaging to proteins," *Biochimica et Biophysica Acta,* pp. 2849-2858, 2013.

[69] A. Fiorati, G. Grassi, A. Graziano and e. al., "Eco-design of nanostructured cellulose sponges for sea-water decontamination from heavy metal ions," *Journal of Cleaner Production* , 2019.

[70] M. Le Gars, A. Delvart, P. Roger, M. Belgacem and J. Bras, "Amidation of TEMPO-oxidized cellulose nanocrystals using aromatic aminated molecules," *Colloid and Polymer Science* , 2020.

[71] P. Mortari Carijo, G. Simoes dos Reis, E. Lima, M. Oliveira and G. Dotto, "Functionalization of corn stover with 3-aminopropyltrietoxysilane to uptake Reactive Red 141 from aqueous solutions," *Environmental Science and Pollution Research* , 2019.

[72] G. Proietto Salanitri, T. Mecca , S. Carroccio, D. Caretti , F. Cunsolo, G. Impellizzeri and S. Dattilo , "From red to green: Smart thiol-porphyrin cryogels combining high mercury efficiency removal and visual material saturation alert," *European Polymer Journal* , 2025.

[73] J. Lebeau, J. Efromson and M. Lynch, "A Review of the Biotechnological Production of Methacrylic Acid," *Frontiers in Bioengineering and Biotechnology* , vol. 8, no. 207, 2020.

[74] M. Paquin, E. Loranger, V. Hannaux , B. Chabot and C. Daneault, "The use of Weissler Method for Scale-up a Kraft Pulp Oxidation by TEMPO-mediated system from a Batch Mode to a Continuous Flow-Through Sonoreactor," *Ultrasonics Sonochemistry* , 2012.

[75] N. Pokhrel , P. K. Vabbina and N. Pala, "Sonochemistry: Science and Engineering," *Ultrasonics Sonochemistry* , 2015.

[76] S. Mishra, J. Thiree, A. Manent, B. Chabot and C. Daneault, "Ultrasound-catalyzed TEMPO-mediated oxidation of native cellulose for the production of nanocellulose: effect of process variables," *Bioresources,* 2011.

[77] S. Koda, T. Kimura, T. Kondo and H. Mitome , "A standard method to calibrate sonochemical efficiency of an individual reaction system," *Ultrasonic Sonochemistry* , 2003.

[78] J. L. Sanchez-Salvador, A. Dunque, D. Lopez-Monte, R. Canadas, Q. Tarres, M. Delgado-Aguilar, A. Blanco and C. Negro, "Process-intensified Production of TEMPO-oxidized Cellulose Nanofibrils: Application to Several Lignocellulosic Feedstocks," *Carbohydrate Polymer Technologies and Applications,* 2026.

[79] J. L. Sanchez-Salvador , A. Blanco , A. Duque , M. J. Negro , P. Manzanares and C. Negro , "Upscaling cellulose oxidation: integrating TEMPO-mediated oxidation in a pilot-plant twin-screw extruder for cellulose nanofibril production," *Carbohydrate Polymer Technologies and Application* , 2024.

[80] J. L. Sanchez-Salvador, H. Xu, A. Balea, A. Blanco and C. Negro , "Enhancement of the production of TEMPO-mediated oxidation cellulose nanofibrils by kneading," *Internation Journal of Biological Macromolecules* , 2024.

[81] J. L. Sanchez-Salvador, H. Xu, A. Balea , E. Fuente, C. Monte, A. Blanco and C. Negro , "Nanocellulose, a Promising Raw Material: Improving the Scalability of TEMPO-mediated Oxidation Process," *IntechOpen.*

[82] F. Franks , "Freeze-drying of bioproducts: putting principles into practice," *European Journal of Pharmaceutics and Biopharmaceutics* , vol. 45, pp. 221-229, 1998.

[83] X. Tang and M. Pikal , "Desing of Freeze-Drying Processes for Pharmaceuticals: Practical Advice," *Pharmaceutical Research* , vol. 21, no. 2, 2004.

[84] H. Xu, J. L. Sanchez-Salvador, A. Blanco, A. Balea and C. Negro, "Recycling of TEMPO-mediated oxidation medium and its effect on nanocellulose properties," *Carbohydrate Polymers,* 2023.

[85] A. Serra, I. Gonzalez, H. Oliver-Ortega, Q. Tarres, M. Delgado-Aguilar and P. Mutjé, "Reducing the Amount of Catalyst in TEMPO-Oxidized Cellulose Nanofibers: Effect on Properties and Cost," *Polymers,* vol. 9, no. 557, 2017.

[86] L. Kuutti, H. Pajari, S. Rovio, J. Kokkonen and M. Nuopponen, "Chemical Recovery in TEMPO Oxidation," *Bioresources* , vol. 11, no. 3, pp. 6050-6061, 2016.

[87] “Watermen Engineers Australia,” [Online]. Available: https://watermanaustralia.com/.

[88] “Huchuan Freeze Dryer Manufacturer,” [Online]. Available: https://huchuan-fd.com/industrial-freeze-dryer/.

List of Figures

List of Tables

Acknowledgments

Desidero ringraziare la mia relatrice, Dr.ssa Laura Riva, per la disponibilità e l'attenzione dimostratomi durante tutto il percorso. Nonostante tutti gli ostacoli, siamo arrivati alla fine.

Ringrazio Arianna per la pazienza e la disponibilità dimostrate in laboratorio, per il tempo dedicatomi e per le chiare spiegazioni della chimica delle reazioni, che altrimenti non avrei ancora capito.

Ringrazio infine tutto l'OSCM Lab per avermi accolto con entusiasmo, rendendo le giornate in laboratorio non solo momenti di crescita e apprendimento, ma anche esperienze piacevoli e stimolanti.